J. Earth Syst. Sci. (2020)129 14
https://doi.org/10.1007/s12040-019-1279-2

Implication of weathering and mineral sorting on rare earth element geochemistry of Pleistocene–Holocene sediments from Cauvery delta, south India

Malik Zubair Ahmad[1,*] and Pramod Singh[2]

[1]*Department of Geology, Satellite Campus Leh, University of Kashmir, Srinagar 194 101, India.*
[2]*Department of Earth Sciences, School of Physical Chemical and Applied Sciences, Pondicherry University, Puducherry 605 014, India.*
**Corresponding author. e-mail: malikzubair.amu@gmail.com*

MS received 7 June 2018; revised 3 August 2019; accepted 29 August 2019

REE analysis of sediments was carried out on representative samples from two cores drilled at Uttrangudi and Porayar locations from Cauvery delta in south India to better understand the patterns and textural and mineralogical control on REEs. Good correlation of REEs and their chondrite normalized ratios $(Gd/Yb \text{ and } La/Yb)_N$ with Ti, Th and Y in both the cores suggest control of Allanite, Titanite and Monazite among heavy minerals on the REE distribution in sediments. Good to strong positive correlation among REEs and Al, Fe, Mg, Ni, Cr, Sc and Co in both the cores suggests partial control of mafic minerals and clay. The Eu/Eu* values show a significant negative correlation with the CIA values, suggesting that the Eu in sediments has been modified to some extent by the process of weathering, affecting its loss and consequently lowering of Eu/Eu* values particularly in Uttrangudi sediments. The correlation of various trace elements with Eu/Eu* suggests that the enrichment of LREE bearing heavy minerals (Allanite, Titanite and Monazite) has resulted in relatively higher increase in LREE and HREE in comparison to Eu that is dominantly held in feldspars, which has further resulted in decreased value of Eu/Eu*.

Keywords. Cauvery; sediment; REE geochemistry; weathering; Eu-anomaly.

1. Introduction

Rare Earth Elements (REEs), due to their unique coherent behaviour, have contributed in understanding the geochemical processes in various fields (Henderson 1984; Taylor and McLennan 1985; Wronkiewicz and Condie 1987; Cullers 1988). The REEs are believed to be carried without any losses and thus retain the signature of their provenance (Frallick and Kronberg 1997; Tripathi and Rajamani 2003; Clift 2016; Dou *et al.* 2016; Bi *et al.* 2017; Maharana *et al.* 2018). The elements of this group for the reason of their similar behaviour are expected not only to preserve their pattern, but also the ratios among them similar to their source (Cullers *et al.* 1987). The chemical composition of elastic sediments is governed by many complex factors, including the average composition of source rocks, weathering processes, transportation processes and diagenesis (Nesbitt 1979; Cullers *et al.* 1987; McLennan 1989; Nesbitt and Young 1996). The REE concentration and their pattern, particularly the Eu anomaly have been found to be interrelated to the variation in grain size and the extent of chemical weathering (Zhao *et al.* 2017). Various studies have highlighted the controls on the REE mobility and fractionation extensively during weathering of different lithology (Sharma

Published online: 20 December 2019

and Rajamani 2000; Vázquez *et al.* 2015; Huang *et al.* 2016; Zhao *et al.* 2017, 2018; Jin *et al.* 2017; Wan *et al.* 2017). Eu systematics has been widely used to discriminate between Archean and Post-Archean sediments as it possibly inherits from the source rocks (Taylor and McLennan 1985; Cullers *et al.* 1987; Hassan *et al.* 1999). Small Eu anomalies are usually attributed to be an input of basic detritus, whereas large anomalies are related to felsic source (McLennan *et al.* 1990; Hassan *et al.* 1999; Cullers 2000). According to Taylor and McLennan (1985), Archean sediments tend to have Eu anomalies higher than 0.85 and at times even higher $(Gd/Yb)_N$ than 2.0. In contrast, the sediments derived from the post Archean rocks tend to have Eu anomaly values lower than 0.85 and a lower $(Gd/Yb)_N$. Also, the Ce anomaly in Archean sediments helps in clarifying about the redox conditions for the evolution of the Earth system. The present study focuses on mainly two aspects of REEs in core sediments: to infer the texture and mineral control on REEs by using various chondrite normalised REE ratio plots and their correlation with certain immobile trace elements, and to highlight the influence of weathering on Eu anomaly in the sediments.

2. Study area

River Cauvery originates from the Brahmagiri ranges of Western Ghats near Talakaveri, Kodagu district of Karnataka. During its initial stretch, the river flows eastward over the Mysore plateau and is joined by several tributaries from north and south (figure 1). The catchment area of the Cauvery includes two major terrains, the northern green stone granite terrain of Dharwar craton and the southern granulite terrain. These terrains constitute a mosaic of several Precambrian terrains separated by several N–S and E–W trending major shear zones (Swaminath and Ramakrishnan 1981; Harris *et al.* 1994; Bhaskar *et al.* 1996; Valdiya 1998; Chadwick *et al.* 2000; Jayananda *et al.* 2000; Meissner *et al.* 2002). These shear zones are supposed to have been reactivated during later periods resulting in the formation of Block Mountains dominantly made up of granulites (Valdiya 1998). The subsequent reactivation of these shear zones during later periods is believed to have resulted in the upliftment and formation of several block mountains, dominantly made up of granulites such as the Nilgiri Hills, Biligirirangan Hills and the Palani–Kodaikanal Hills (Harris *et al.* 1994; Valdiya 1998; Raith *et al.* 1999). The Dharwar craton comprises vast areas of Tonalite Trondzehmite gneisses (TTG – commonly known as peninsular gneisses) which is further subdivided into the western (WDC) and eastern blocks (EDC) based on the nature and abundance of greenstone belts, degree of regional metamorphism and melting as well as the nature and age of their gneissic basement rocks (Swaminath *et al.* 1976; Chadwick *et al.* 1981; Jayananda *et al.* 2000). The Southern Granulitic Terrain (SGT), forming part of Cauvery catchment is delineated by the crustal scale shear zones that subdivided it into two major blocks, the Northern Granulite Block (NGB) and the Southern Granulite Block (SGB). The northern part of SGT in the Cauvery catchment area consists of Meso-Neo Archean charnockite massifs forming Nilgiri hills massif, Biligirirangan hills massif and the Shevroy hills massif (Rajesh 2012) whereas, the SGB consists of Palani–Kodaikanal massif of Madurai Block (MB). On the western margin of the delta, Precambrian gneisses are exposed, overlain by Cretaceous to Recent sediments. The Cauvery forms a moderate sized delta that commences at Tiruchirapalli. The radiocarbon dates obtained from the borehole peat from 20 m depth in the delta, suggested that the Holocene sediments are 3 m thick about 50 km inland and about 30 m thick near the present shoreline (Sadakata 1980). The present Cauvery delta has been formed by erosion and later deposition over the older sedimentary rocks of the Cauvery Basin. The underlying older sediments of Cretaceous and Tertiary age were deposited in the intra-cratonic rift basin that was further divided into a number of subparallel horsts and grabens, trending in a general NE–SW direction. The basin is believed to have come into existence due to divergent tensional block faulting of continental crust and subsidence during Late Jurassic age and records a sedimentation history till recent with alternate transgressive and regressive cycles (Radhakrishna 1983). The major part of the basin experiences a semiarid climate except for the uppermost reaches of the catchment that has humid climate. The drainage basin on an average receives annual rainfall of 1100 mm mainly during the North East (NE) monsoon season. The NE monsoon shares 60% of the annual rainfall in the coastal part, while in the regions located in the interior part it shares 40–50% of the average annual rainfall (Balachandran *et al.* 2006). The annual mean temperature of

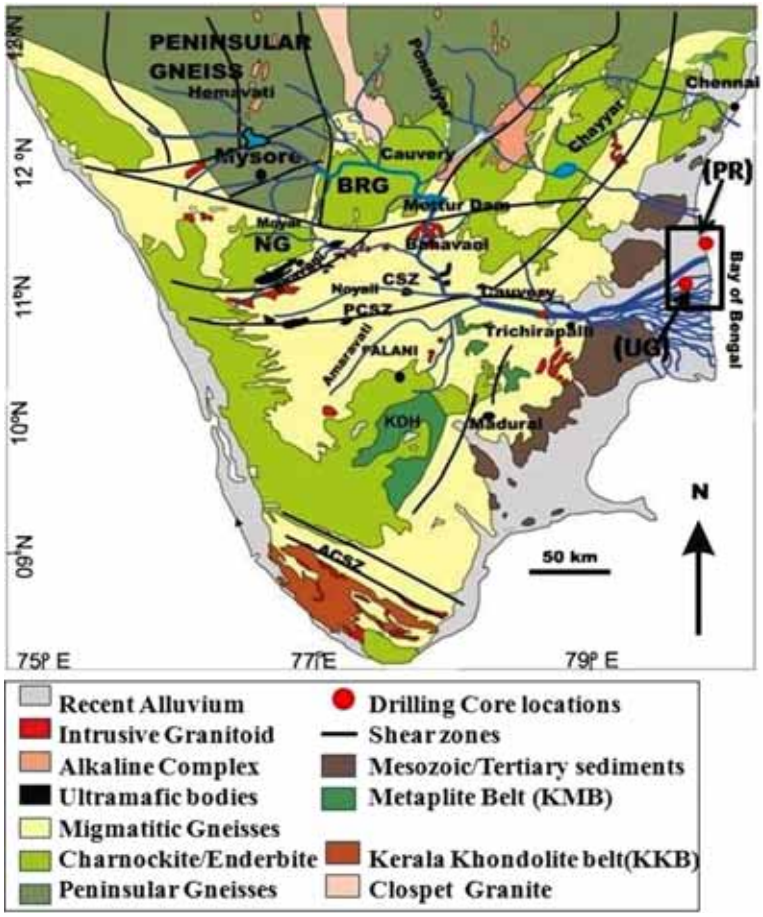

Figure 1. Geological map of Cauvery Basin modified after Santosh *et al.* (2009).

these basins is 26°C; however, in summer the maximum temperature reaches up to 41°C (May) and during winter (January) it goes down to 13.5°C. In the present study, two cores of Uttrangudi (UG) and Porayar (PR) from distinct delta geomorphic setting were analyzed. The core from Uttrangudi (UG) was collected around 25 km inland from the Bay of Bengal coast near Tiruvarur area (N10°39′17.7″; E79°39′42.2″). At Porayar (PR), core was collected from around 2 km inland from Bay of Bengal, located north of Karaikal region (N11°01′17.8″; E79°50′42.6″). The local elevation of this site is 2 m above mean sea level (figure 1).

3. Methodology

Two cores from Uttrangudi (UG) and Porayar (PR) were retrieved by diamond/Tungsten core drilling bit involving a double barrel core tube from Cauvery delta. The length of two cores is 31.5 and 26.5 m, respectively. For REE analysis, based on textural variation, 34 samples were collected from Uttrangudi and 26 from Porayar core. The samples were labelled according to depth and stored in plastic bags. The grain size of core sediments was measured by laser particle size analyzer (Cillas 1190). The powdered bulk samples were used for mineralogical analysis by using PANalytical X'pert PRO X-ray Diffractometer (XRD) equipped with θ–θ type Goniometer. The bulk minerals were identified by standard procedures (Dixon *et al.* 1977; Nesse *et al.* 1996). Clay minerals were separated from other rock forming minerals in the bulk samples for clay mineral analysis. Clay minerals have an average grain size of <2 m and were separated based on their differential settling velocity when suspended in a column of water. The separation procedure was based on the method described by Hardy and Tucker (1988). For REEs, samples were digested by NaOH and Na_2O_2 fusion method in nickel crucible. REE separation and

pre-concentration were done using HNO_3 and HCl cation exchange resin (Bio-Rad AG50-X8) column (Singh and Rajamani 2001). All the elements were analyzed using a JY ICP-AES (ULTIMA 2) using international and laboratory working standards and subsequently further analyzed by ICP-AES. For major and trace element determination, standard B-solution procedure of Shapiro and Brannock (1962) was followed (Singh and Rajamani 2001). Among trace elements, Sc, Co, U, Th and Rb were analyzed by (Thermo Scientific, Xseries-2), ICP-MS. Rock standards AMH and DGH supplied by the Wadia Institute of Himalaya Geology, Dehradun (Saini *et al.* 1998) and internal rock standards 21-6, 22-22, 22-7 and VM-9 were calibrated using the USGS rock standards BHVO-1, RGM-1, BCR-2 and STM-1 for calibration of ICP-AES for major and trace element analysis. The element analysis in ICP-MS was carried by using international USGS standards AGV-2, SCO-1, GSP-2, W-2a, SDC-1, and BHVO-2 for calibration. Rare Earth Elements were determined on pre-concentrated solutions after calibrating the ICP-AES with the standards AMH, DGH, 86-89 and 90-57. REE values of the internal rock standards were previously determined using isotope dilution technique at Stony Brook, New York, USA (Krogstad *et al.* 1991). Analyzing the standards AMH and DGH as unknown checked these values. The precision of major, trace and REEs were checked by replicate analysis of the samples. Both precision and accuracy for major elements are better than 2% and for trace elements and REEs, precision and accuracy are better than 2% and 5% respectively. For low REE samples (<5× chondrite) the precision was 5–10% for Ce and Nd. The precision on repeated measurement for Th, Sc, Co, U Ta and, Nb is <3% and the accuracy is better than 10%. Radiocarbon dating was carried on same cores by Srikanth (2012) and Singh *et al.* (2015). The detailed methodology for conventional technique is given in Srikanth (2012). Apart from radiocarbon dating, three dates for Uttrangudi core were obtained by optically stimulated luminescence (OSL) techniques by Alappat *et al.* (2010). Age dates are calibrated with Int. Cal 09 of Calib 611 (Stuiver and Reimer 1993). Calculation of Chemical Index of Alteration, CIA (Nesbitt and Young 1982) using molar proportion of Al_2O_3, CaO, Na_2O and K_2O was done on carbonate free basis (Singh and Rajamani 2001).

4. Results

4.1 *Lithology*

The borehole lithology of two cores (figures 2 and 3) is described here. The Uttrangudi borehole consists of sediments of middle to late Pleistocene and Holocene age and the Porayar borehole consists mostly of Holocene age sediments resting unconformably over older Tertiary/Cretaceous sedimentary rocks. The litho-stratigraphic boundaries are recognized by change of lithology and physical characteristics of sediments, such as color and texture. Both Pleistocene and Holocene sediments of Uttrangudi are composed of clayey silt, silt, sandy silt, silty sand and gravelly to pebbly sand units. The sediments range in colour from light brown, dark brown, grayish, greenish gray, grayish brown, grayish black to red. In some places dispersed mottling is present, whereas some bands are completely mottled. The Porayar core sediments are grey to brownish colour mud, to silty sand units containing dispersed calcrete nodules. Rootlets and traces of rootlets are present along with decomposed vegetal matter and plant fragments in the Porayar sediments except at depth greater than 20 m whereas, in Uttrangudi sediments it is limited to around top 7 m. Foraminiferal tests and fragments of molluscan shells are present in the Porayar sediments. Based upon texture, 31.5 m core obtained from Uttrangudi location was divided into eight fluvial units. The bottom six units (unit VIII–III), from 30.75 to 7.5 m depth comprise of the Pleistocene deposits and the top 2 units, i.e., 7 m upward constitutes of Holocene deposits (figure 2). The 26.5 m deep Porayar core was obtained from north of the axial part of the delta. The bottom ~7 m of the core is believed to be Mio-Pliocene in age over which unconformably lie the 20 m section of sediments deposited mainly during the Holocene period. On the basis of texture and colour, the Porayar core was divided into six units (figure 3).

4.2 *Minerology*

Quartz and feldspar are the dominant minerals present in both core sediments. Other minerals identified by X-ray diffraction include micas/clay minerals (muscovite-illite) with occasional occurrence of hornblende and pyroxene. The clay minerals present are Smectite, Illite and Kaolinite in varying proportions. In Uttrangudi core, clay mineralogy consists of Smectite (84–47%), Illite (9–34%) and Kaolinite (6–21%). The three

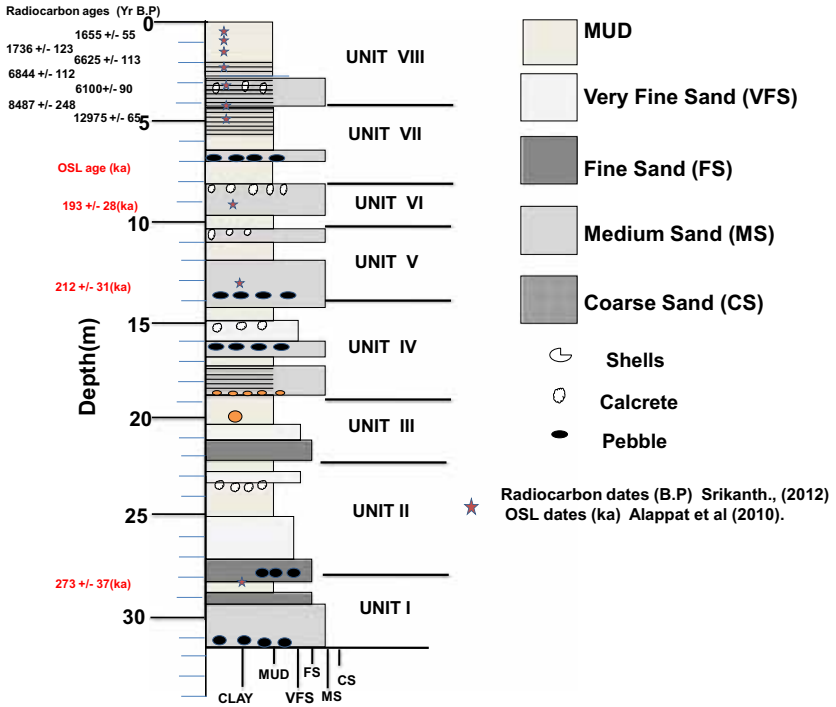

Figure 2. Borehole lithology and stratigraphic position of radiocarbon dated levels for Uttrangudi (UG) core from distal part of Cauvery delta.

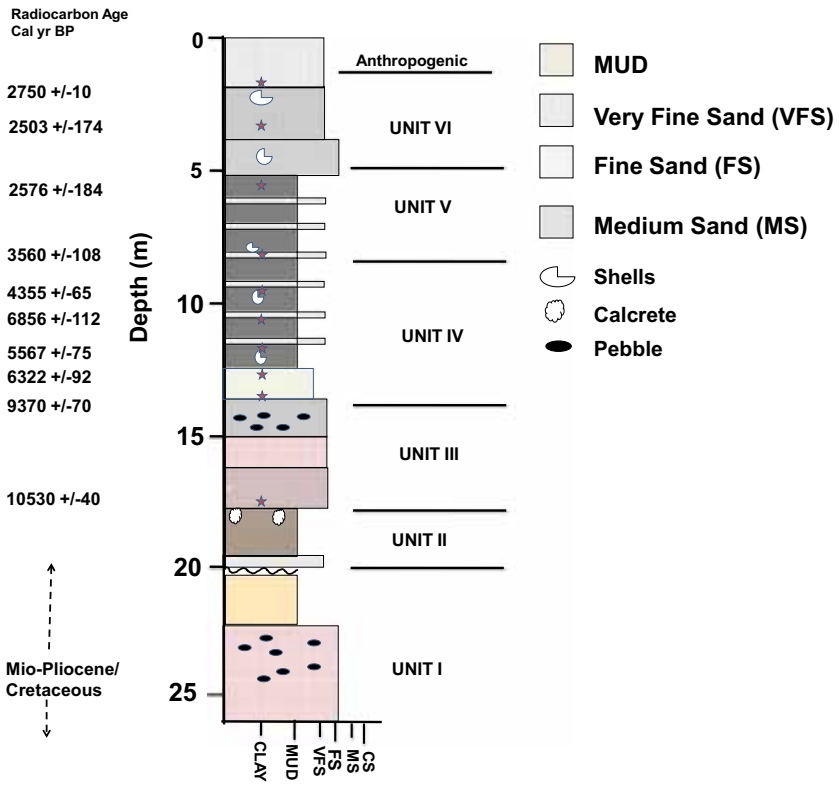

Figure 3. Borehole lithology and stratigraphic position of radiocarbon dated level for Porayar (PR) core from central marginal part of delta plain.

minerals are present throughout the entire depth of the core though in varying proportions. The clay mineralogy of the Porayar sediments shows presence of Smectite, Kaolinite and Illite with abundance in descending order, although in varying proportion throughout the studied core. Illite,

with other clay minerals, is present throughout the Porayar core unlike the Uttrangudi core sediments; indicating the input from the same source.

4.3 *Geochmistry*

The data of the major, trace and REEs for sediments from Uttrangudi and Porayar core are given in tables 1(a and b) and 2(a and b), respectively. The number associated with the sample denotes the depth in cm. The depth-wise plot of individual REEs and ∑REE along with the texture are shown in figures 4 and 5, respectively. The total REE (∑REE) concentration of sediments from Uttrangudi core ranges from 52 to 246 ppm with an average value of 157 ppm. The average ∑REE concentration of sediments from Porayar site is 136 ppm, ranging from 46 to 215 ppm, except one sample at 8.3 m having value of 270 ppm. This may be due to lower SiO_2 content (56.2%) and high CIA value (76.7) in this sample. The variation and concentration of REEs is higher in the Uttrangudi sediments. In spite of the variations in the abundance of REEs, the patterns remained somewhat similar in all the samples. The uniformity of patterns is to some extent by heavy minerals and ferro-magnesian contributing differentially to individual samples. The range of $(Ce/Yb)_N$, $(Ce/Sm)_N$ and $(Gd/Yb)_N$ ratios of Uttrangudi sediments is 7.4–10.9, 2.5–4.0 and 1.4–2.7, respectively, except for three samples at 22.45, 23.28 and 23.88 m that have lower $(Ce/Yb)_N$ values of 3.5, 6.01 and 3.7, respectively and $(Gd/Yb)_N$ value of 1. In case of Porayar sediments, their $(Ce/Yb)_N$, $(Ce/Sm)_N$ and $(Gd/Yb)_N$ ratio ranges are 5.3–8.3, 2.2–3.3 and 1.4–2.1, respectively (table 2).

The Uttrangudi sediments exhibit slight to negligible negative Eu anomalies ranging between 0.79 and 0.97, whereas Porayar sediments exhibit negative to slightly positive Eu anomalies ranging between 0.7 and 1.2 except one sample, which shows value of 1.6. SiO_2 in Uttrangudi core sediments exhibits strong negative correlation with almost all the major and trace elements (Ti, Fe, Mg, K, Na, P, Ni, Cr and Y) except Ca, Mn, Ba and Sr (table 3).

5. Discussion

5.1 *Textural and mineralogical control on REEs*

Chemical composition of the clastic sediments is determined by of a number of geological factors. This includes the intensity of chemical weathering, rate of sediment supply, sorting and post-depositional changes in addition to the source rock chemistry (Alvarez and Roser 2007; Huntsman *et al.* 2009). Each of these factors must be evaluated for drawing conclusions on the nature of source rocks and tectonics of the region. In the following discussion, the compositional features of sediments that result from chemical weathering and fluvial process of sorting was considered. The depth-wise plot of individual REE and ∑REE along with texture for both Uttrangudi and Porayar sediments are shown in figures 4 and 5. All the REEs are observed to show good positive correlation amongst them as also with silt (%) and negative correlation with sand (%). It is observed that the finer sediments are having higher concentration of REEs. The good positive correlation of various REEs with silt and clay and their negative correlation with sand percentage suggest that in the studied sediments majority of the REE holding mineral phases are concentrated in the silt fraction and REEs are also held in clays. Thus, the first order of variation in concentration of REEs in the studied sediments is because of the varying percentage of sand, which acts as a diluting agent for REEs. The above observation has been reported in other studies also where REEs are depleted in sand-fraction because of dilution by quartz and carbonate minerals (Gouveia *et al.* 1993; Vital *et al.* 1999; Shou *et al.* 2002). Similarly, Singh and Rajamani (2001) have also observed that nearly 70–80% of REEs are present in finer fractions (silt and clay) in the floodplain sediments of Cauvery River.

Major and trace element data suggest that the mafic minerals and even feldspar are fine grained and the overall variation in their chemistry is influenced by processes of fluvial sorting. Good positive correlation of Al_2O_3 with K_2O and moderate correlation with Na_2O indicate that feldspar (sodic and pottasic) and muscovite are reduced in size and are mostly fine-grained. The strong correlation among Fe, Mg, Ti, Ni and Cr indicates that these elements are held in mafic minerals and their good correlation with Al_2O_3 and mud percentage indicate that like REEs, they are also held in finer fraction. Similarly, good correlation of P_2O_5 and Y with Al_2O_3 and mud, suggests their enrichment in finer fraction (table 4).

Comparison of REEs from both the studied cores with other compositional variables of the

Table 1. *(a) Major and trace element concentration of samples from Uttrangudi borehole. (b) Rare earth element (REE) in (ppm) adundances along with their chondrite normalized ratios of samples from Uttrangudi borehole.*

	Depth	Si	Al	Ti	Fe	Mg	Mn	Ca*	Na*$_2$O	K_2O	P
(a)											
UG 83	83	61.0	21.0	1.1	10.1	1.9	0.2	1.4	1.6	1.6	0.1
UG 113	113	62.0	22.5	1.0	9.3	1.8	0.2	0.7	1.1	1.4	0.1
UG 185	185	55.3	23.8	1.1	10.6	2.5	0.2	1.1	3.4	2.0	0.2
UG 220	220	56.9	23.5	1.0	10.9	2.6	0.2	0.8	2.1	1.8	0.2
UG 240	240	56.3	23.2	1.0	10.5	2.4	0.2	1.4	2.9	1.9	0.2
UG 260	260	61.5	19.9	1.0	8.3	2.3	0.2	1.6	3.1	2.0	0.2
UG 280	290	64.4	17.6	1.4	9.0	1.8	0.2	1.7	2.4	1.4	0.2
UG 313	319	89.3	6.3	0.6	2.1	0.3	0.1	0.5	0.4	0.4	0.0
UG 380	380	86.1	7.3	0.9	3.1	0.5	0.1	1.0	0.4	0.5	0.0
UG 392	392	85.7	7.7	1.0	3.2	0.7	0.1	0.5	0.5	0.6	0.0
UG 419	419	76.6	11.9	0.9	5.1	1.6	0.1	1.3	1.2	1.3	0.0
UG 427	427	70.7	15.5	1.0	6.4	1.9	0.1	1.3	1.4	1.6	0.1
UG 457	457	74.8	14.2	0.9	5.7	1.7	0.2	0.8	0.4	1.3	0.0
UG 477	477	74.9	12.0	1.0	5.4	1.6	0.1	1.5	1.8	1.6	0.1
UG 526	526	71.2	15.1	0.9	6.3	1.8	0.1	1.6	1.5	1.4	0.1
UG 546	546	70.8	16.1	0.9	6.8	1.9	0.1	1.0	0.9	1.4	0.1
UG 566	566	68.8	16.3	0.9	8.1	1.9	0.2	1.2	1.2	1.3	0.1
UG 650	650	81.5	10.3	0.7	4.5	1.2	0.1	0.7	0.4	0.6	0.1
UG 815	815	66.1	18.1	1.0	9.3	2.2	0.2	1.1	1.0	0.9	0.1
UG 825	835	68.7	16.5	0.9	8.0	2.1	0.1	1.4	1.2	0.9	0.1
UG 855	855	77.5	11.7	0.6	3.4	1.1	0.1	2.3	2.2	1.1	0.0
UG 1010	1010	78.8	12.2	0.8	4.9	1.2	0.1	0.8	0.7	0.4	0.0
UG1200	1200	74.6	14.7	1.0	6.0	1.2	0.1	1.0	0.8	0.8	0.0
UG 1430	1430	81.6	11.1	0.9	4.6	0.9	0.1	0.2	0.1	0.4	0.0
UG 1510	1510	80.7	11.4	0.8	4.1	0.7	0.1	0.8	0.6	0.8	0.0
UG 1703	1703	83.8	9.6	0.7	4.1	0.5	0.0	0.5	0.3	0.4	0.0
UG1912	1912	78.3	13.1	0.9	5.5	0.9	0.4	0.4	0.2	0.3	0.0
UG 2098	2098	79.8	12.5	0.9	5.4	0.4	0.0	0.1	0.1	0.6	0.1
UG 2138	2138	83.8	10.3	0.8	4.2	0.3	0.0	0.1	0.1	0.3	0.1
UG 2245	2245	83.8	10.1	0.8	4.5	0.3	0.0	0.0	0.0	0.5	0.1
UG 2328	2328	79.3	13.2	0.8	5.1	1.0	0.0	0.0	0.1	0.4	0.1
UG 2388	2490	80.7	12.3	0.8	4.7	1.1	0.0	0.1	0.1	0.2	0.0
UG 2490	2490	78.5	13.1	0.9	5.2	1.1	0.0	0.4	0.5	0.2	0.0
UG 2760	2760	81.8	10.3	0.7	4.7	0.8	0.0	0.8	0.8	0.6	0.0

	Ba	Sr	Cr	Ni	Sc	Co	Th	U	Y	Zr	Rb
(a)											
UG 83	796.6	239.6	426.9	193.9	19.8	34.8	18.9	3.1	40.9	123.7	69.6
UG 113	745.4	238.7	352.6	156.1	21.3	34.6	20.2	2.9	40.8	108.5	82.8
UG 185	908.9	259.8	446.3	177.8	15.7	29.4	14.3	2.1	43.4	290.2	80.8
UG 220	770.0	231.9	446.3	178.0	39.3	74.4	16.5	3.1	44.9	207.7	195.9
UG 240	879.8	255.4	356.5	172.3	34.1	79.3	14.7	2.8	42.2	247.1	176.7
UG 260	886.9	327.5	363.6	125.2	27.6	57.1	14.1	2.2	35.8	231.5	147.0
UG 280	534.7	246.1	189.9	54.1	17.5	30.2	11.7	1.4	20.0	124.3	96.0
UG 313	462.1	124.1	93.6	37.4	9.3	46.4	8.0	0.8	15.9	84.6	40.3
UG 380	407.1	152.7	94.8	36.1	12.8	35.0	9.9	1.0	15.5	82.4	59.4
UG 392	564.9	157.5	83.3	38.6	10.0	33.5	10.6	1.1	21.2	130.0	55.9
UG 419	1095.8	282.5	204.1	67.3	15.7	41.7	13.3	2.2	34.9	105.2	93.9
UG 427	968.5	310.3	187.8	82.3	21.0	38.2	14.3	2.0	24.4	123.2	109.7
UG 457	624.6	253.8	167.2	73.4	19.4	47.0	13.7	2.1	22.5	100.6	114.0
UG 477	631.5	288.8	252.7	76.9	21.4	33.7	12.5	1.9	22.2	106.9	97.4
UG 526	593.4	319.2	213.0	130.5	21.5	41.7	14.0	2.8	25.7	154.4	114.4
UG 546	555.2	269.1	197.2	98.5	23.2	37.6	12.9	3.0	23.8	127.8	133.8

Table 1. *(Continued.)*

	Ba	Sr	Cr	Ni	Sc	Co	Th	U	Y	Zr	Rb
UG 566	552.0	301.1	196.0	140.1	22.5	39.7	12.4	3.6	33.4	142.6	128.5
UG 650	535.0	194.8	94.9	82.4	16.9	33.8	10.6	2.7	28.0	108.9	73.5
UG 815	802.8	300.4	244.6	179.2	26.6	66.9	14.2	3.3	29.1	114.3	88.1
UG 825	501.4	379.2	170.1	114.8	21.7	37.7	12.2	1.9	28.7	120.2	75.7
UG 855	648.5	441.6	109.2	49.3	10.9	25.1	5.6	0.9	18.2	99.8	52.3
UG 1010	368.3	191.1	143.9	88.1	17.6	40.5	12.4	1.5	28.8	134.1	54.3
UG1200	832.0	280.7	224.7	84.8	19.0	32.6	11.6	1.6	30.0	128.0	59.7
UG 1430	660.8	161.5	171.3	66.7	15.0	40.8	10.1	1.2	25.1	95.1	43.2
UG 1510	500.6	203.2	181.4	57.3	11.9	25.2	10.1	0.7	15.3	136.2	50.5
UG 1703	266.1	139.9	153.3	45.2	12.5	23.0	9.3	0.8	15.8	112.5	38.4
UG1912	917.2	135.5	235.2	84.0	17.2	42.8	10.3	1.2	24.9	114.8	38.7
UG 2098	95.7	46.3	112.4	78.5	14.5	33.0	10.1	1.4	33.0	361.5	26.1
UG 2138	101.1	45.2	170.9	64.8	N.D	N.D	N.D	N.D	28.0	353.3	N.D
UG 2245	53.9	99.8	173.7	105.9	14.4	15.0	9.9	1.2	20.6	43.6	24.9
UG 2328	58.9	38.3	150.2	53.3	N.D	N.D	N.D	N.D	9.4	240.7	N.D
UG 2388	99.9	67.0	214.8	79.6	20.8	24.1	13.1	1.3	12.9	257.5	41.5
UG 2490	107.6	54.0	236.7	82.8	15.3	21.6	8.5	0.8	13.2	227.3	28.8
UG 2760	313.0	154.9	149.3	48.7	N.D	N.D	N.D	N.D	22.2	211.6	N.D

	Depth	La	Ce	Nd	Sm	Eu	Gd	Dy	Yb	Lu	TREE
(b)											
UG 83	83	54.7	115.9	44.9	9.3	2.1	7.8	6.3	3.4	0.5	244.9
UG 113	113	54.8	115.3	46.7	9.4	2.2	7.9	6.5	3.4	0.5	246.6
UG 185	185	50.8	104.3	43.8	8.8	1.9	7.3	5.9	3.2	0.5	226.6
UG 220	220	48.3	103.2	41.4	8.8	1.9	7.2	6.0	3.2	0.5	220.5
UG 240	240	46.3	102.1	41.3	8.9	2.0	7.3	6.2	3.3	0.5	217.8
UG 260	260	52.5	106.5	45.9	8.8	2.1	7.4	5.7	3.4	0.6	232.8
UG 280	290	28.0	57.9	22.2	4.4	1.1	3.6	2.9	1.9	0.2	122.2
UG 313	319	25.0	54.9	19.3	4.0	1.0	3.2	2.5	1.6	0.4	111.7
UG 380	380	21.1	42.3	16.3	3.4	0.8	2.8	2.3	1.5	0.2	90.7
UG 392	392	29.4	54.6	21.9	4.5	1.0	3.7	3.1	1.9	0.3	120.4
UG 419	419	45.0	77.1	35.7	7.0	1.8	6.6	5.2	2.7	0.4	181.5
UG 427	427	34.9	82.8	29.1	5.9	1.4	4.9	3.7	2.3	0.3	165.5
UG 457	457	38.8	90.4	32.3	6.5	1.5	4.9	3.9	2.2	0.4	180.9
UG 477	477	45.0	89.3	39.0	7.7	1.8	6.2	4.8	2.8	0.6	197.1
UG 526	526	39.8	85.9	33.2	6.7	1.6	5.1	4.1	2.4	0.5	179.3
UG 546	546	33.8	73.0	27.6	5.6	1.4	4.4	3.6	2.1	0.3	151.8
UG 566	566	41.5	89.7	34.5	7.4	1.8	6.2	5.0	2.8	0.6	189.4
UG 650	650	37.8	69.3	29.8	5.9	1.4	5.0	3.6	2.1	0.4	155.3
UG 815	815	36.8	100.1	32.1	6.9	1.7	6.2	4.9	3.1	0.6	192.4
UG 825	835	43.3	72.3	34.7	6.6	1.7	5.8	4.3	2.4	0.4	171.4
UG 855	855	23.2	44.4	18.0	3.6	1.1	3.2	2.5	1.4	0.2	97.6
UG 1010	1010	44.8	113.0	36.7	7.6	1.8	6.4	5.0	3.0	0.6	218.8
UG1200	1200	46.4	81.6	40.0	7.2	1.8	6.0	4.5	2.8	0.5	190.9
UG 1430	1430	36.7	77.1	29.4	5.9	1.4	5.2	3.8	2.4	0.5	162.3
UG 1510	1510	23.9	61.6	18.4	3.7	0.9	3.1	2.4	1.8	0.4	116.2
UG 1703	1703	24.4	57.4	18.5	3.8	0.9	3.0	2.2	1.6	0.4	112.1
UG1912	1912	43.7	101.0	36.3	7.8	1.8	6.6	5.4	3.3	0.7	206.6
UG 2098	2098	15.9	50.7	13.2	3.2	0.7	2.8	2.1	1.4	0.3	90.4
UG 2138	2138	28.4	75.1	22.9	4.9	1.1	4.3	3.5	2.2	0.4	142.8
UG 2245	2245	18.3	31.5	14.3	3.1	0.7	3.1	2.8	2.4	0.6	76.9
UG 2328	2328	14.0	24.6	8.0	1.5	0.4	1.4	1.4	1.1	0.2	52.6

Table 1. *(Continued.)*

	Depth	La	Ce	Nd	Sm	Eu	Gd	Dy	Yb	Lu	TREE
UG 2388	2490	21.9	17.8	10.1	1.9	0.4	1.6	1.3	1.3	0.3	56.4
UG 2490	2490	35.7	34.8	21.7	3.3	0.7	2.3	1.8	1.2	0.2	101.8
UG 2760	2760	70.9	85.8	48.6	8.4	2.2	7.4	4.7	2.2	0.4	230.5

	La/Yb	Ce/Yb	Eu*	La/Sm	GD/Yb	Ce/Sm	Silt(%)	Sand(%)	MUD(%)	CIA
(b)										
UG 83	10.9	8.9	0.7	3.7	1.8	3.0	50.8	47.1	52.9	75.2
UG 113	10.9	8.9	0.8	3.7	1.9	3.0	60.5	36.5	63.6	83.4
UG 185	10.6	8.4	0.7	3.6	1.8	2.9	61.9	35.2	64.8	71.1
UG 220	10.3	8.6	0.7	3.4	1.8	2.8	81.5		100.0	77.3
UG 240	9.5	8.1	0.7	3.2	1.8	2.8	45.3	53.1	46.9	71.3
UG 260	10.6	8.3	0.8	3.7	1.8	2.9	62.3	35.8	64.3	66.2
UG 280	9.9	7.9	0.8	3.9	1.5	3.1	37.0	61.7	38.3	67.0
UG 313	10.6	9.0	0.8	3.9	1.6	3.3	26.5	72.1	27.9	76.1
UG 380	9.5	7.4	0.8	3.9	1.5	3.0	20.6	78.6	21.4	70.3
UG 392	10.4	7.5	0.8	4.1	1.6	2.9	23.3	75.7	24.3	77.0
UG 419	11.5	7.6	0.8	4.0	2.0	2.6	50.9	46.8	53.2	67.3
UG 427	10.2	9.4	0.8	3.7	1.7	3.4	50.9	46.8	53.2	70.6
UG 457	12.1	10.9	0.8	3.7	1.8	3.3	66.1	31.4	68.6	79.4
UG 477	11.0	8.5	0.8	3.6	1.8	2.8	57.3	40.5	59.6	61.8
UG 526	11.4	9.5	0.8	3.7	1.7	3.1	58.6	29.1	70.9	68.7
UG 546	10.7	9.0	0.8	3.7	1.7	3.1	67.9	28.3	71.7	76.7
UG 566	10.0	8.3	0.8	3.5	1.8	2.9	56.8	40.3	59.7	73.9
UG 650	12.2	8.6	0.8	4.0	1.9	2.8	60.5	36.5	63.6	80.4
UG 815	8.0	8.5	0.8	3.3	1.6	3.5	71.6	26.0	74.0	79.2
UG 825	12.4	8.0	0.8	4.1	2.0	2.6	67.9	29.5	70.5	75.4
UG 855	11.3	8.3	1.0	4.1	1.9	3.0	42.8	55.6	44.5	56.7
UG 1010	10.2	9.9	0.8	3.7	1.7	3.6	85.6	10.5	89.5	79.7
UG1200	11.3	7.7	0.8	4.0	1.8	2.7	65.6	31.7	68.3	79.4
UG 1430	10.6	8.6	0.8	3.9	1.8	3.2	78.9	19.0	81.0	91.1
UG 1510	9.2	9.2	0.8	4.1	1.4	4.0	46.8	51.4	48.6	77.3
UG 1703	10.4	9.5	0.8	4.0	1.5	3.7	60.5	36.5	63.6	83.3
UG1912	9.1	8.1	0.8	3.5	1.6	3.1	88.8	8.7	91.3	90.5
UG 2098	7.7	9.6	0.7	3.1	1.6	3.8	40.2	58.7	41.3	92.9
UG 2138	8.8	9.0	0.7	3.6	1.6	3.7	49.5	49.0	51.0	94.8
UG 2245	5.2	3.5	0.7	3.7	1.0	2.5	58.4	40.0	60.0	94.2
UG 2328	8.9	6.0	0.8	5.8	1.1	3.9	48.7	49.8	50.2	95.3
UG 2388	7.9	3.7	0.7	4.8	1.0	2.3	56.9	41.4	58.6	94.6
UG 2490	20.6	7.8	0.8	6.7	1.6	2.5	65.8	31.9	68.1	87.3
UG 2760	21.8	10.2	0.8	5.3	2.7	2.5	60.3	37.7	62.3	75.0

sediments, indicates that these sediments show some similarities and differences. The REEs in Uttrangudi sediments show good positive correlation with Th and Y; moderate positive correlation with Al, Fe, Mg, Mn, Ni, Cr, Sc, Co, and poor correlation with Ti (table 3). In contrast the REEs in Porayar sediments show strong positive correlation with Al, Fe, Mg, Ti, Th, Y, Ni, Cr, Sc and Co, and a moderate correlation with Mn (table 4). Good to moderate correlation with Al, Fe, Mg, Ni, Cr, Sc and Co in both the cores suggests the control of mafic minerals and clay. Strong correlation of REEs with Ti, Th and Y in Porayar sediments suggests the control of Allanite, Titanite, Monazite and Zircon. In contrast, poor correlation of REEs with Ti and their good correlation with Th and Y in Uttrangudi sediments suggest control of Monazite and Zircon.

Table 2. *(a) Major and trace element concentration of samples from Porayar borehole. (b) Rare earth element (REE) abundances in (ppm) along with their chondrite normalized ratios of Porayar borehole.*

	Depth	SiO_2	Al_2O_3	TiO_2	Fe_2O_3	MgO	MnO	Ca*O	$Na*_2O$	K_2O	P_2O_5
(a)											
PR 283	283	74.6	13.2	0.2	2.7	1.3	0.03	2.6	2.7	2.2	0.25
PR 329	329	74.0	13.9	0.5	3.4	1.3	0.04	2.6	2.3	1.9	0.07
PR 426	426	75.3	14.4	0.2	1.5	0.8	0.03	2.6	2.8	2.0	0.28
PR 548	548	61.0	20.0	0.8	7.4	2.9	0.09	2.8	2.4	2.3	0.33
PR 645	645	66.5	17.1	0.6	5.4	2.3	0.08	3.0	2.4	2.1	0.55
PR 775	775	63.4	19.4	0.8	7.0	2.5	0.10	2.6	2.0	2.2	0.17
PR 831	831	56.2	22.8	1.0	11.3	3.5	0.15	1.3	1.1	2.5	0.18
PR 842	842	65.0	18.5	0.8	8.8	2.7	0.12	1.1	1.0	1.9	0.10
PR 945	945	61.8	19.6	0.9	8.7	3.1	0.10	1.9	1.4	2.4	0.14
PR 1029	1029	80.2	10.9	0.5	2.9	1.3	0.06	1.8	1.3	1.0	0.13
PR 1170	1170	72.2	14.8	0.6	5.2	1.9	0.05	1.7	1.3	2.0	0.09
PR 1226	1226	75.6	13.7	0.6	4.3	1.7	0.04	1.7	1.2	1.0	0.10
PR 1279	1279	76.8	12.6	0.5	3.1	1.2	0.05	2.1	1.7	1.9	0.04
PR 1351	1351	78.1	12.6	0.5	2.8	1.0	0.04	2.2	1.7	1.0	0.10
PR 1453	1453	72.1	15.5	0.7	3.3	1.3	0.04	2.8	2.2	2.2	0.03
PR 1483	1483	72.6	14.4	0.6	3.8	1.3	0.04	3.1	2.4	1.6	0.04
PR 1573	1573	71.5	14.7	0.7	4.0	1.5	0.05	3.3	2.5	1.7	0.05
PR 1643	1643	73.9	13.1	0.7	3.9	1.4	0.05	3.1	2.2	1.5	0.07
PR 1718	1718	80.3	9.4	0.5	2.6	1.0	0.06	1.8	2.6	1.7	0.06
PR 1785	1785	73.9	13.2	0.6	4.7	1.7	0.14	2.0	1.5	2.2	0.04
PR 1833	1833	62.3	20.4	0.9	8.8	3.0	0.06	1.0	1.0	2.3	0.14
PR 1863	1863	62.6	19.9	0.9	9.2	2.7	0.07	1.1	1.2	2.3	0.05
PR 1923	1923	65.4	18.8	0.8	6.7	2.1	0.07	1.8	1.9	2.4	0.06
PR 1953	1953	69.2	17.0	0.7	4.5	1.5	0.06	2.2	2.4	2.4	0.05
PR 2170	2170	78.6	11.6	0.5	3.9	1.2	0.02	1.5	1.4	1.2	0.02
PR 2348	2348	70.3	14.2	0.7	5.1	1.7	0.04	3.8	2.5	1.7	0.04

	Ba	Sr	Cr	Ni	Sc	Co	Th	U	Zr	Y	Rb
(a)											
PR 283	688.4	385.8	105.3	84.6	7.6	13.7	3.8	0.7	46.7	12.0	74.2
PR 329	626.7	360.9	83.8	32.2	11.6	19.7	5.9	0.8	215.9	12.6	85.2
PR 426	786.4	470.3	52.2	68.6	4.3	6.9	1.6	0.3	16.5	5.6	67.4
PR 548	615.8	381.2	250.7	130.2	13.4	23.7	6.3	1.0	73.4	26.9	101.7
PR 645	717.8	456.7	192.8	109.0	12.3	23.9	5.0	0.8	53.4	22.5	93.6
PR 775	603.3	372.3	223.2	119.4	16.9	26.3	8.6	1.3	68.5	26.0	133.8
PR 831	414.2	232.2	333.8	158.1	27.7	44.4	12.6	2.1	65.3	41.4	204.3
PR 842	345.8	199.5	332.9	125.1	19.7	34.0	8.9	1.5	160.9	31.1	134.7
PR 945	482.1	323.1	245.5	135.8	21.7	35.9	9.8	1.8	55.9	26.6	157.8
PR 1029	590.2	345.6	103.2	70.6	9.4	16.5	5.5	0.7	27.8	12.4	77.5
PR 1170	525.0	316.7	157.2	88.0	13.8	22.2	7.1	1.0	38.9	15.9	106.9
PR 1226	566.7	344.2	154.8	90.8					38.1	15.8	
PR 1279	630.9	395.2	100.1	72.7	9.0	15.5	5.6	1.1	25.7	14.3	77.2
PR 1351	698.4	393.2	108.5	83.8	10.3	17.0	4.7	1.5	35.8	14.1	69.7
PR 1453	679.5	465.6	139.4	47.8	11.5	22.4	5.7	2.8	600.8	23.9	62.5
PR 1483	744.2	513.8	145.4	60.4					174.8	25.0	
PR 1573	768.4	489.0	150.0	62.5	12.4	16.7	6.5	0.8	199.5	21.7	68.0
PR 1643	709.2	463.2	159.5	113.5	12.6	15.7	7.2	0.8	604.0	24.4	47.8
PR 1718	592.7	291.5	91.7	27.2					536.4	14.4	
PR 1785	734.6	349.4	166.3	64.8	14.1	29.7	6.9	1.6	160.6	25.4	86.2
PR 1833	457.5	237.1	312.9	121.5					196.5	28.8	
PR 1863	599.1	279.4	296.0	112.6	24.2	35.9	8.8	1.6	172.8	37.7	135.5
PR 1923	510.4	321.2	220.8	85.7	19.0	31.6	7.5	1.2	185.1	25.1	121.2

Table 2. *(Continued.)*

	Ba	Sr	Cr	Ni	Sc	Co	Th	U	Zr	Y	Rb
PR 1953	638.8	411.8	242.5	63.2	14.5	23.1	6.9	0.9	191.0	18.2	90.1
PR 2170	308.8	242.1	120.8	37.8	12.3	14.4	4.7	0.6	151.3	11.7	63.8
PR 2348	475.9	331.6	192.7	70.2	12.6	23.5	6.9	0.9	234.0	20.7	73.7

	Depth	La	Ce	Nd	Sm	Eu	Gd	Dy	Yb	Lu
(b)										
PR 283	283	16.5	28.7	12.1	2.7	1.0	2.2	1.8	1.1	0.2
PR 329	329	31.3	47.4	23.4	4.0	1.3	4.0	3.3	2.1	1.0
PR 426	426	12.5	19.6	7.9	1.8	0.8	1.4	1.2	0.7	0.1
PR 548	548	52.3	96.5	40.1	7.0	2.1	6.7	5.8	3.1	0.4
PR 645	645	44.4	90.4	35.4	7.1	1.8	6.0	5.0	3.2	0.5
PR 775	775	47.2	89.6	39.2	7.2	1.8	7.6	5.5	3.1	0.6
PR 831	831	60.2	124.6	51.9	9.6	2.4	9.2	7.3	4.3	0.7
PR 842	842	37.1	73.8	31.4	6.5	1.4	5.9	4.4	2.6	0.4
PR 945	945	42.6	83.6	36.6	7.3	1.9	6.1	4.9	2.7	0.6
PR 1029	1029	18.3	34.1	14.2	3.1	0.9	2.5	2.0	1.1	0.2
PR 1170	1170	28.3	55.4	22.8	5.0	1.4	4.0	3.0	2.0	0.5
PR 1226	1226	28.2	50.1	22.2	4.9	1.4	4.0	3.1	2.2	0.5
PR 1279	1279	21.0	36.2	16.2	3.8	1.2	3.0	2.2	1.6	0.4
PR 1351	1351	21.2	40.4	16.5	3.5	1.1	2.7	2.4	1.5	0.3
PR 1453	1453	30.0	49.6	23.7	5.1	1.6	4.5	3.4	2.4	0.5
PR 1483	1483	30.4	53.8	23.7	5.3	1.6	4.5	3.5	2.4	0.6
PR 1573	1573	28.8	54.1	24.2	4.9	1.2	3.9	3.1	2.0	0.4
PR 1643	1643	36.3	61.4	25.8	5.0	1.5	4.1	3.0	2.3	0.2
PR 1718	1718	21.2	37.7	16.1	3.7	1.1	3.0	2.2	1.7	0.4
PR 1785	1785	30.3	47.0	25.2	5.2	1.3	4.6	3.6	1.8	0.3
PR 1833	1833	37.0	83.9	30.2	6.5	1.7	5.6	4.4	2.8	0.6
PR 1863	1863	49.4	95.8	41.9	8.6	2.4	7.9	5.8	3.2	0.6
PR 1923	1923	35.9	68.8	28.7	6.0	1.6	4.9	4.0	2.2	0.4
PR 1953	1953	29.3	56.2	24.2	4.8	1.3	4.1	3.3	1.9	0.4
PR 2170	2170	27.6	58.5	23.2	4.8	1.2	3.8	3.2	2.0	0.3
PR 2348	2348	40.4	77.6	33.8	6.8	1.7	5.5	4.5	2.7	0.5

	TREE	La/Yb	Ce/Yb	Eu*	La/Sm	GD/Yb	Ce/Sm	Clay(%)	Silt(%)	Sand(%)	Mud	CIA
(b)												
PR 283	66.2	10.3	6.9	1.2	3.8	1.6	2.6	3.3	28.8	68.0	32.0	53.4
PR 329	117.7	10.0	5.8	1.0	4.9	1.5	2.9	0.8	23.0	76.2	23.8	56.9
PR 426	46.0	13.0	7.9	1.6	4.5	1.7	2.7	0.7	10.3	89.0	11.0	55.2
PR 548	214.0	11.4	8.1	0.9	4.6	1.7	3.3	1.2	46.8	52.0	48.0	63.1
PR 645	193.8	9.5	7.5	0.8	3.9	1.5	3.1	1.1	41.1	57.9	42.1	59.5
PR 775	201.9	10.3	7.6	0.7	4.1	2.0	3.0	5.3	63.4	31.3	68.7	65.3
PR 831	270.2	9.4	7.5	0.8	3.9	1.7	3.1	14.2	83.3	2.4	97.6	76.7
PR 842	163.7	9.6	7.4	0.7	3.6	1.8	2.7	2.2	58.0	39.8	60.2	76.1
PR 945	186.2	10.8	8.2	0.9	3.6	1.8	2.8	11.4	67.0	21.6	78.4	69.9
PR 1029	76.5	11.4	8.2	1.0	3.6	1.9	2.6	7.2	45.6	47.2	52.8	62.8
PR 1170	122.3	9.8	7.4	1.0	3.6	1.7	2.7	10.4	56.1	33.5	66.5	66.4
PR 1226	116.6	8.9	6.1	1.0	3.6	1.5	2.5	7.0	46.5	46.5	53.5	68.7
PR 1279	85.5	9.1	6.1	1.1	3.5	1.5	2.3	6.3	44.9	48.8	51.2	59.4
PR 1351	89.7	9.5	7.0	1.0	3.7	1.4	2.7	3.4	49.1	47.5	52.5	61.7
PR 1453	120.8	8.4	5.3	1.0	3.7	1.5	2.4					58.3
PR 1483	125.9	8.6	5.9	1.0	3.6	1.5	2.4	2.6	41.4	56.0	44.0	55.8
PR 1573	122.7	9.9	7.2	0.9	3.7	1.6	2.7	2.8	38.8	58.4	41.6	55.1
PR 1643	139.5	10.5	6.9	1.0	4.6	1.4	3.0	1.5	35.2	63.4	36.6	54.7

Table 2. *(Continued.)*

	TREE	La/Yb	Ce/Yb	Eu*	La/Sm	GD/Yb	Ce/Sm	Clay(%)	Silt(%)	Sand(%)	Mud	CIA
PR 1718	87.1	8.7	6.0	1.0	3.6	1.5	2.5	4.9	47.8	47.3	52.7	49.8
PR 1785	119.3	11.6	7.0	0.8	3.6	2.1	2.2	6.6	77.8	15.5	84.5	60.9
PR 1833	172.7	9.0	7.9	0.9	3.6	1.6	3.1	7.0	92.9	0.1	99.9	77.1
PR 1863	215.5	10.4	7.8	0.9	3.6	2.0	2.7					75.6
PR 1923	152.4	11.3	8.3	0.9	3.8	1.8	2.8	5.8	74.4	19.8	80.2	67.5
PR 1953	125.4	10.3	7.6	0.9	3.8	1.7	2.8	4.1	58.5	37.4	62.6	61.6
PR 2170	124.6	9.2	7.5	0.8	3.6	1.5	2.9	0.8	28.6	70.7	29.4	64.6
PR 2348	173.6	10.0	7.4	0.8	3.7	1.6	2.7	1.9	54.8	43.3	56.7	57.6

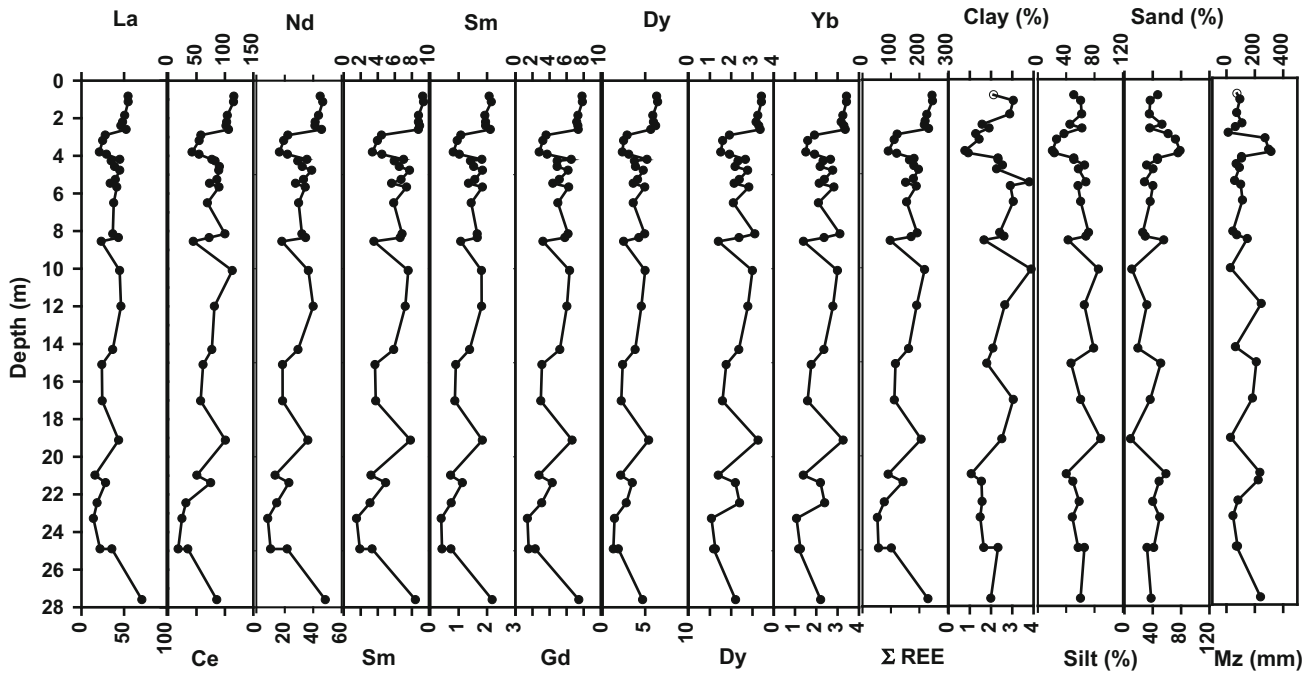

Figure 4. The depth-wise plot of individual REEs and total REE (∑REE) along with the texture for Uttrangudi core. All the REE's are observed to show good positive correlation among them and with silt (%). It is also observed that the finer sediments are having higher concentration of REE.

To understand the mineralogical control on REEs in the core sediments, REE ratios $(Gd/Yb)_N$ and $(La/Yb)_N$ are plotted against each other, with total REE concentration (∑ REE) and also with Th and Ti. These plots are used in order to understand the mineralogical control on REEs in the core sediments. It is understood that among the various LREE-enriched mineral phases, addition of Monazite would lead to increase in total REE, LREE and $(La/Yb)_N$ ratios. In addition, it also leads to increase in $(Gd/Yb)_N$ ratios of the sediments. Similarly, in case of the Uttrangudi sediments, the REEs are observed to follow the above relation (figure 6a, b, d). This is further supported by the positive correlation among Gd_N and $(Gd/Yb)_N$ as well as among $(La/Yb)_N$ and $(Gd/Yb)_N$ (figure 6e), thus corroborating the control of monazite over the REE concentration in Uttrangudi sediments. Similar relations are observed for the Porayar sediments (figure 7a–i). Better positive correlation of Th with ∑REE also supports the control of Monazite on REEs in the studied sediments. The variation in $(Ce/Yb)_N$ ratios in the samples, is largely due to the variation in $(Ce/Sm)_N$ ratios, as can be seen by greater variation in $(Ce/Sm)_N$ values ranging between 2.46 and 4.05 in case of Uttrangudi and narrow range (1.42–2.73) of $(Gd/Yb)_N$ (table 2). Similar and prominent pattern of $(Ce/Sm)_N$ ratio (range 2.17–3.31) and $(Gd/Yb)_N$ ratio (range 1.41–2.11) is observed in case of Porayar core. Thus the observed variation in $(Ce/Yb)_N$ ratios is due to the variable accumulation of mafic and heavy minerals enriched in LREEs.

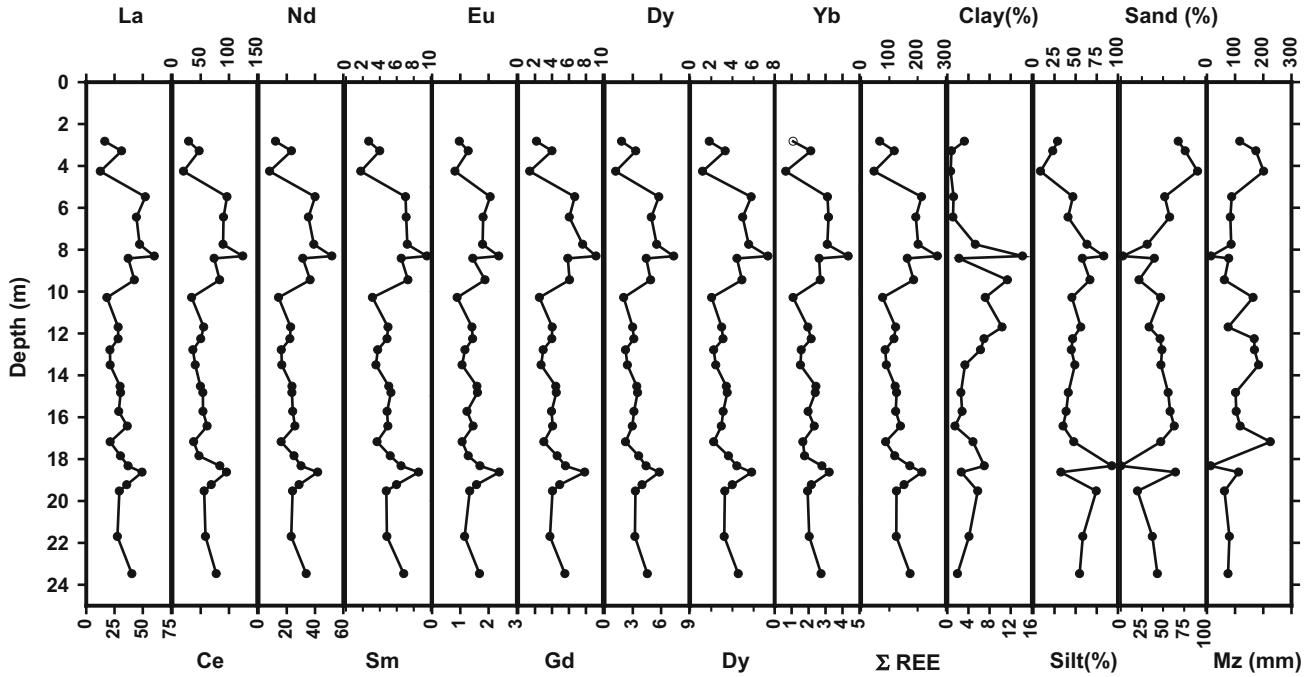

Figure 5. The depth-wise plot of individual REE and total REE (∑REE) along with the texture in sediments from Porayar borehole. All the REE's are observed to show good positive correlation among them and with silt (%).

It is also observed that Ti and Y also show good positive correlation with ΣREE (figures 6g, h, 7g and h). This suggests that other LREE enriched mineral phases particularly Titanite and Allanite have also contributed to the REE concentrations in the sediments. Strong positive correlation of Y with $(Gd/Yb)_N$ ratio (figures 6i and 7i) indicates the major contribution of Y from LREE bearing phase such as Allanite. Since in case of HREE bearing minerals particularly zircon, the Yb concentration is expected to be higher which may lower $(Gd/Yb)_N$ ratio. This should in turn result in the development of negative correlation of $(Gd/Yb)_N$ with $(La/Yb)_N$. Since Y is also a major element present in zircon, it should also show negative correlation of $(Gd/Yb)_N$, if it is primarily contributed by zircon which is not the case in studied sediments (figures 6c, i, 7c and i). The above discussion shows that the LREE enriched heavy mineral phases along with the mafic minerals have largely controlled the REE concentration and pattern in the sediments from both the studied locations.

5.2 *Influence of weathering on Eu anomaly*

The chondrite normalized REE patterns are less fractionated for mafic rocks, whereas they are more fractionated in felsic rocks. The chondrite normalized plots of REEs in sediments from both the core are almost parallel to each other and exhibit similarly fractionated patterns (figure not included) with the $(Ce/Yb)_N$ ratio of ∼8.2 although with large variations in their abundance. Similar patterns for individual samples may imply either uniform source rocks and/or efficient mixing of source lithologies during transport and deposition processes (McLennan 1989). The more fractionated nature of LREE and flatter HREE along with slight negative to positive Eu anomaly, suggests that the sediments have been derived from a rock of intermediate composition. In the present study, the sediments from both Uttrangudi and Porayar sites are plotted in Eu/Eu* vs. $(Gd/Yb)_N$ diagram (figure 8a and b). Sediments from both the locations show higher Eu/Eu* values of more than 0.72 and up to ∼1.6. The Eu/Eu* value of Uttrangudi sediments ranges between 0.73 and 0.84, except one sample which shows a higher value of 0.96. The range of Eu/Eu* values in Porayar sediments is between 0.7 and 1.2, except one sample which shows a value of 1.6. In general, it is observed that Eu/Eu* values are higher in Porayar samples in comparison to Uttrangudi sediments.

The $(Gd/Yb)_N$ ratio shows a similar range between 1.4 and 2 in both sediment cores except three samples from Uttrangudi which show much lower value of around 1.0. It should be noted that in Eu/Eu* vs. $(Gd/Yb)_N$ diagram (figure 8), all the samples plot above the field of upper continental crust (UCC) and post-Archaean Australian shale (PAAS).

Table 3. *Correlation matrix for major and trace element concentration and ∑REE of samples from Uttrangudi borehole.*

	SiO_2	Al_2O_3	TiO_2	Fe_2O_3	MgO	MnO	Ca*O	Na^*_2O	K_2O	P_2O_5	*Ba*	*Sr*	*Cr*	*Ni*	*Sc*	*Co*	Th	U	Y	Rb	La	Ce	Nd	Sm	Eu	Gd	Dy	Yb	Lu	∑REE
SiO_2	1.00																												
Al_2O_3	−0.98	1.00																											
TiO_2	−0.73	0.68	1.00																										
Fe_2O_3	−0.97	0.97	0.76	1.00																									
MgO	−0.93	0.88	0.63	0.88	1.00																								
MnO	−0.58	0.54	0.48	0.56	0.59	1.00																							
Ca*O	−0.53	0.39	0.37	0.39	0.62	0.38	1.00																						
Na^*_2O	−0.82	0.73	0.56	0.70	0.78	0.44	0.77	1.00																					
K_2O	−0.86	0.78	0.62	0.75	0.84	0.50	0.71	0.88	1.00																				
P_2O_5	−0.80	0.76	0.70	0.78	0.67	0.36	0.38	0.80	0.72	1.00																			
Ba	−0.59	0.52	0.44	0.50	0.66	0.78	0.61	0.61	0.69	0.35	1.00																		
Sr	−0.56	0.45	0.31	0.43	0.68	0.46	0.90	0.67	0.71	0.29	0.71	1.00																	
Cr	−0.85	0.88	0.57	0.84	0.72	0.47	0.25	0.67	0.69	0.67	0.50	0.27	1.00																
Ni	−0.85	0.87	0.52	0.88	0.76	0.51	0.27	0.54	0.62	0.56	0.44	0.36	0.83	1.00															
Sc	−0.75	0.75	0.44	0.76	0.79	0.45	0.26	0.50	0.61	0.59	0.38	0.34	0.66	0.72	1.00														
Co	−0.52	0.50	0.25	0.52	0.59	0.63	0.24	0.40	0.46	0.40	0.54	0.29	0.41	0.50	0.77	1.00													
Th	−0.75	0.77	0.61	0.77	0.70	0.41	0.17	0.39	0.64	0.47	0.47	0.26	0.74	0.76	0.65	0.42	1.00												
U	−0.71	0.69	0.42	0.73	0.77	0.46	0.35	0.40	0.65	0.42	0.46	0.47	0.54	0.79	0.73	0.55	0.76	1.00											
Y	−0.76	0.76	0.50	0.76	0.65	0.56	0.28	0.57	0.67	0.57	0.60	0.39	0.72	0.79	0.62	0.56	0.72	0.71	1.00										
Rb	−0.73	0.67	0.45	0.66	0.81	0.48	0.52	0.66	0.82	0.64	0.54	0.55	0.53	0.54	0.84	0.74	0.57	0.73	0.58	1.00									
La	−0.55	0.53	0.32	0.54	0.57	0.45	0.36	0.47	0.50	0.24	0.57	0.42	0.58	0.51	0.56	0.46	0.71	0.63	0.64	0.53	1.00								
Ce	−0.65	0.63	0.43	0.63	0.63	0.68	0.38	0.49	0.61	0.33	0.70	0.49	0.62	0.65	0.55	0.59	0.71	0.66	0.79	0.56	0.81	1.00							
Nd	−0.65	0.62	0.41	0.62	0.65	0.57	0.43	0.56	0.62	0.33	0.68	0.52	0.65	0.60	0.59	0.52	0.71	0.66	0.76	0.59	0.97	0.91	1.00						
Sm	−0.69	0.66	0.44	0.67	0.68	0.66	0.43	0.57	0.65	0.38	0.72	0.52	0.68	0.67	0.62	0.59	0.73	0.70	0.82	0.62	0.92	0.95	0.98	1.00					
Eu	−0.64	0.59	0.39	0.61	0.65	0.63	0.48	0.55	0.63	0.32	0.73	0.58	0.59	0.60	0.58	0.56	0.68	0.69	0.77	0.61	0.93	0.93	0.98	0.99	1.00				
Gd	−0.66	0.63	0.42	0.65	0.65	0.64	0.41	0.55	0.62	0.37	0.72	0.52	0.65	0.66	0.59	0.58	0.71	0.69	0.83	0.57	0.91	0.94	0.97	0.99	0.99	1.00			
Dy	−0.72	0.70	0.48	0.71	0.68	0.70	0.40	0.57	0.66	0.43	0.74	0.50	0.72	0.73	0.61	0.59	0.74	0.70	0.87	0.59	0.85	0.94	0.94	0.98	0.96	0.98	1.00		
Yb	−0.69	0.68	0.51	0.70	0.64	0.70	0.32	0.52	0.61	0.44	0.70	0.46	0.72	0.75	0.60	0.55	0.72	0.66	0.83	0.52	0.75	0.91	0.86	0.92	0.89	0.93	0.96	1.00	
Lu	−0.31	0.32	0.17	0.35	0.26	0.49	0.02	0.15	0.22	0.12	0.39	0.20	0.44	0.54	0.38	0.35	0.34	0.38	0.51	0.17	0.46	0.65	0.56	0.62	0.60	0.64	0.65	0.78	1.00
∑REE	−0.65	0.63	0.42	0.64	0.65	0.63	0.41	0.53	0.61	0.33	0.70	0.50	0.65	0.64	0.58	0.57	0.73	0.68	0.78	0.58	0.93	0.97	0.98	0.99	0.98	0.98	0.96	0.90	0.62	1.00

Table 4. *Correlation matrix for major and trace element concentration and ∑REE of samples from Porayar borehole.*

	SiO_2	Al_2O_3	TiO_2	Fe_2O_3	MgO	MnO	Ca*O	Na^*_2O	K_2O	P_2O_5	Mz	Ba	Sr	Cr	Ni	Sc	Co	Th	Y	Rb	La	Ce	Nd	Sm	Eu	Gd	Dy	Yb	Lu	∑REE
SiO_2	1.00																													
Al_2O_3	−0.98	1.00																												
TiO_2	−0.77	0.73	1.00																											
Fe_2O_3	−0.92	0.89	0.84	1.00																										
MgO	−0.93	0.89	0.79	0.97	1.00																									
MnO	−0.66	0.61	0.62	0.73	0.74	1.00																								
Ca*O	0.20	−0.27	−0.26	−0.49	−0.40	−0.34	1.00																							
Na^*_2O	0.26	−0.31	−0.47	−0.57	−0.52	−0.41	0.81	1.00																						
K_2O	−0.74	0.73	0.41	0.56	0.57	0.50	−0.10	0.08	1.00																					
P_2O_5	−0.31	0.30	−0.20	0.12	0.29	0.18	0.19	0.27	0.24	1.00																				
Mz	0.80	−0.76	−0.69	−0.74	−−0.76	−0.65	0.04	0.23	−0.67	-0.15	1.00																			
Ba	0.33	−0.32	−−0.45	−0.58	-0.50	−0.25	0.61	0.64	−0.05	0.21	0.12	1.00																		
Sr	0.31	−0.29	−0.38	−0.60	−0.52	−0.40	0.80	0.71	−0.11	0.19	0.14	0.88	1.00																	
Cr	−0.89	0.87	0.85	0.95	0.91	0.69	−0.43	−0.50	0.55	0.09	−0.79	−0.52	−0.53	1.00																
Ni	−0.80	0.79	0.58	0.80	0.86	0.63	−0.28	−0.44	0.40	0.43	−0.67	−0.29	−0.30	0.76	1.00															
Sc	−0.82	0.81	0.87	0.95	0.87	0.71	−0.55	−0.61	0.49	−0.14	−0.69	−0.55	−0.64	0.89	0.66	1.00														
Co	−0.83	0.81	0.83	0.93	0.88	0.82	−0.50	−0.58	0.58	−0.06	−0.79	−0.49	−0.61	0.88	0.64	0.95	1.00													
Th	−0.76	0.72	0.90	0.89	0.83	0.75	−0.40	−0.59	0.43	−0.22	−0.73	−0.51	−0.56	0.84	0.66	0.93	0.90	1.00												
Y	−0.84	0.79	0.88	0.88	0.83	0.74	−0.27	−0.41	0.53	0.00	−0.80	−0.29	−0.33	0.88	0.69	0.89	0.89	0.87	1.00											
Rb	−0.84	0.85	0.66	0.91	0.89	0.75	−0.57	−0.55	0.58	0.12	−0.64	−0.51	−0.63	0.79	0.74	0.88	0.88	0.83	0.73	1.00										
La	−0.88	0.81	0.83	0.86	0.87	0.66	−0.10	−0.30	0.51	0.23	−0.67	−0.37	−0.32	0.81	0.71	0.81	0.79	0.79	0.86	0.72	1.00									
Ce	−0.90	0.84	0.83	0.91	0.91	0.64	−0.20	−0.37	0.49	0.26	−0.67	−0.47	−0.41	0.86	0.75	0.83	0.80	0.79	0.85	0.76	0.98	1.00								
Nd	−0.88	0.82	0.85	0.89	0.89	0.69	−0.16	−0.36	0.51	0.18	−0.69	−0.43	−0.38	0.84	0.70	0.86	0.84	0.84	0.88	0.77	0.99	0.98	1.00							
Sm	−0.87	0.81	0.87	0.91	0.89	0.67	−0.22	−0.42	0.49	0.13	−0.72	−0.46	−0.41	0.86	0.69	0.88	0.87	0.84	0.91	0.77	0.96	0.97	0.98	1.00						
Eu	−0.87	0.82	0.81	0.85	0.84	0.56	−0.14	−0.31	0.54	0.17	−0.71	−0.30	−0.26	0.79	0.68	0.82	0.80	0.76	0.88	0.72	0.95	0.93	0.95	0.95	1.00					
Gd	−0.88	0.83	0.84	0.90	0.89	0.71	−0.22	−0.39	0.53	0.16	−0.70	−0.41	−0.40	0.85	0.70	0.87	0.86	0.84	0.90	0.80	0.97	0.97	0.99	0.98	0.95	1.00				
Dy	−0.89	0.84	0.82	0.90	0.90	0.70	−0.20	−0.37	0.53	0.21	−0.69	−0.43	−0.40	0.84	0.70	0.85	0.85	0.81	0.87	0.79	0.98	0.98	0.99	0.98	0.95	0.99	1.00			
Yb	−0.83	0.77	0.83	0.84	0.83	0.60	−0.13	−0.33	0.44	0.18	−0.63	−0.41	−0.33	0.79	0.65	0.80	0.78	0.79	0.86	0.70	0.96	0.96	0.96	0.96	0.94	0.96	0.96	1.00		
Lu	−0.48	0.46	0.53	0.49	0.48	0.26	−0.13	−0.23	0.33	−0.06	−0.29	−0.27	−0.25	0.37	0.15	0.53	0.54	0.53	0.45	0.51	0.58	0.53	0.58	0.56	0.60	0.61	0.60	0.65	1.00	
∑REE	−0.89	0.83	0.84	0.90	0.90	0.66	−0.17	−0.35	0.51	0.23	−0.68	−0.44	−0.38	0.85	0.73	0.84	0.82	0.81	0.87	0.76	0.99	1.00	1.00	0.98	0.95	0.98	0.99	0.97	0.57	1.00

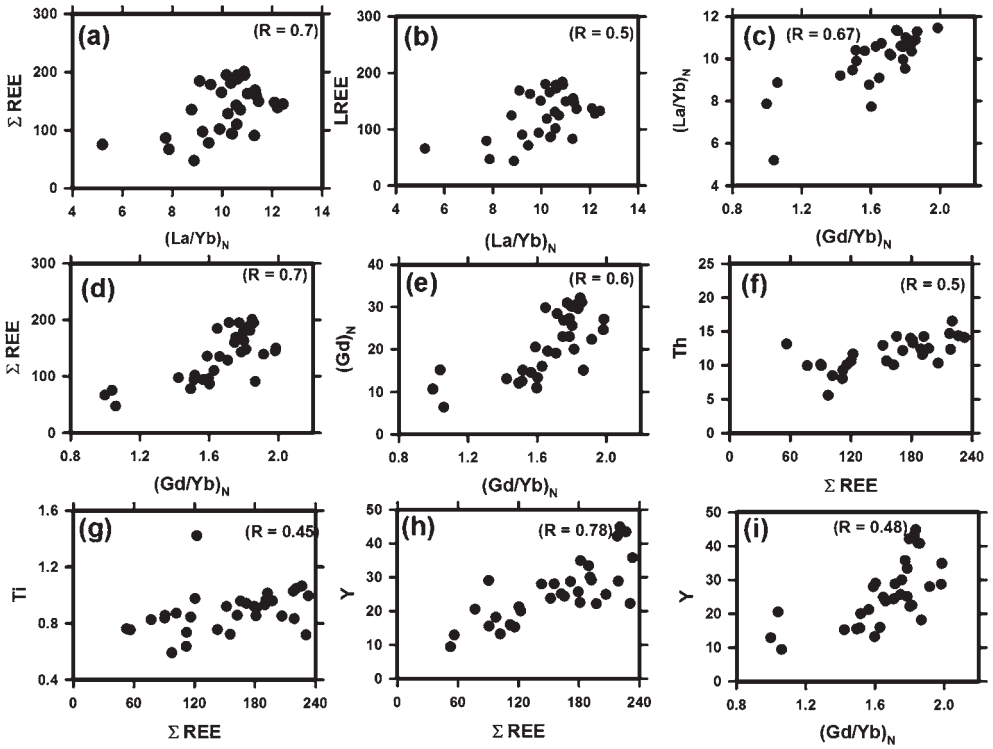

Figure 6. The binary plot of Ti, Th and Y with total REE, LREE and chondrite normalised ratios. The above correlations indicate control of Monazite, Allanite and Titanite on the REE distribution in sediments from Uttrangudi as discussed in the text.

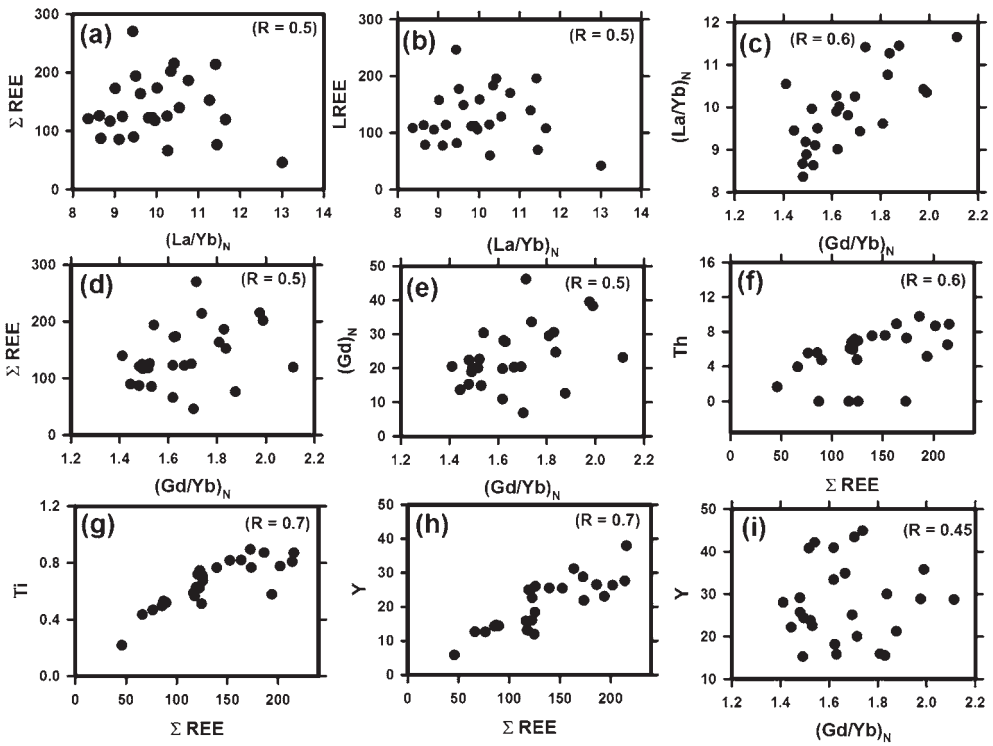

Figure 7. The binary plot of Ti, Th and Y with total REE, LREE and chondrite normalised ratios. The above correlations indicate control of Monazite, Allanite and Titanite on the REE distribution in sediments from Porayar borehole sediments as discussed in the text.

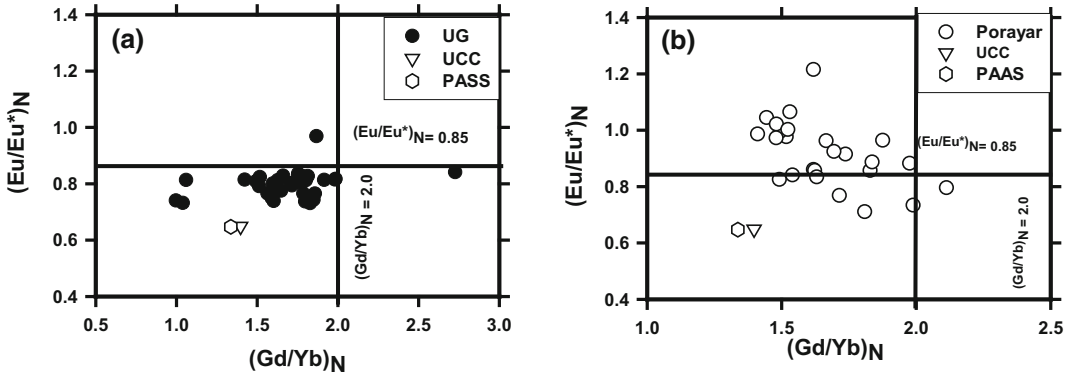

Figure 8. In the above plot, sediments from both Uttrangudi and Porayar sites are plotted in the Eu/Eu* vs. $(Gd/Yb)_N$ diagram (a and b). Sediments from both the locations show higher Eu/Eu* values of more than 0.72 up to ∼1.6. The Eu/Eu* value of Uttrangudi sediments ranges between 0.73 and 0.84 except one sample, which shows higher value of 0.96. The range of Eu/Eu* values in Porayar sediments is between 0.7 and 1.2, except one sample which shows value of 1.6. It should be noted that all samples plot above the field of upper continental crust (UCC) and post-Archaean Australian shale (PAAS). This is expected as the catchment of the Cauvery River dominantly comprises of Archean lithologies. It is noted that although the Uttrangudi and Porayar sediments show an overlap in the above diagram, they differ primarily in their Eu/Eu* values.

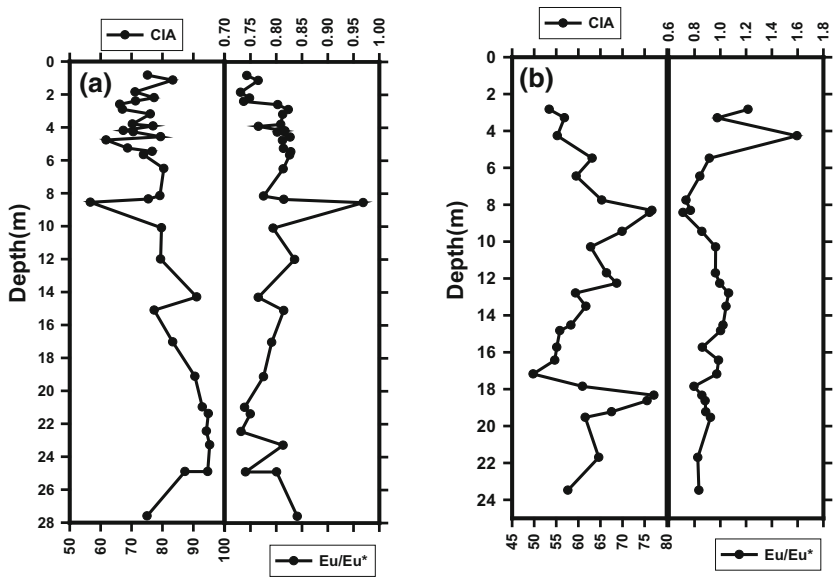

Figure 9. The depth wise variation in Eu/Eu* values of (**a**) Uttrangudi and (**b**) Porayar sediments along with their CIA (Chemical Index of Weathering) from both the locations. Significant anti correlation Eu/Eu* with the CIA values, particularly in (**a**) suggest that the Eu in sediments have been modified by the process of weathering effecting its loss and lowering of Eu/Eu* values.

This is expected, as the catchment of the Cauvery dominantly comprises of Archean lithology. It is to be noted that although the Uttrangudi and Porayar sediments show an overlap in the diagram, they differ primarily in their Eu/Eu* values (figure 9).

Furthermore, to evaluate the effect of weathering on Eu, the depth-wise variation in Eu/Eu* values of sediments along with their CIA (chemical index of alteration) from both the locations were plotted (figure 8a and b). The CIA is a well-established weathering proxy. The ratio is based on the relative mobility of Na, K and Ca in water relative to Al, which normally concentrates in the weathered rock. The CIA values were calculated using the method of Nesbitt and Young (1982) as shown below.

$$\mathrm{CIA} = [\mathrm{Al_2O_3}/(\mathrm{Al_2O_3} + \mathrm{CaO^*} + \mathrm{Na_2O} + \mathrm{K_2O})] \times 100$$

where CaO* is the amount of CaO incorporated in the silicate fraction of rocks.

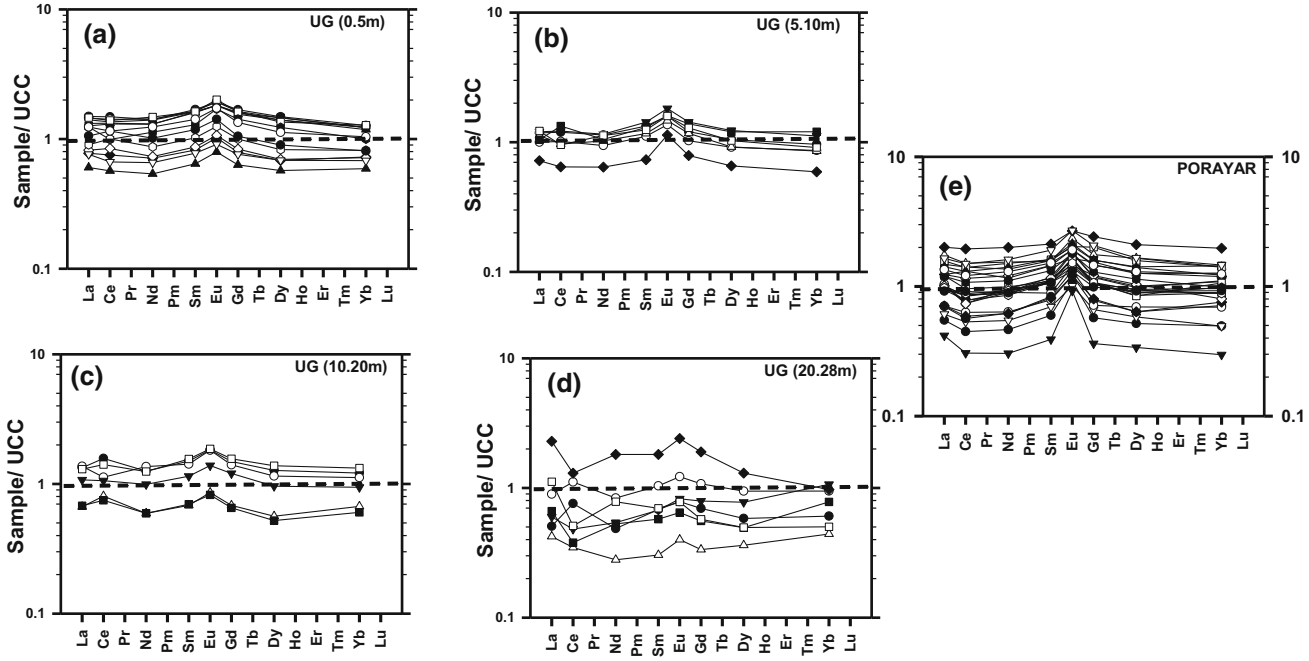

Figure 10. The above plot shows UCC normalized REE pattern of Uttrangudi (**a–d**) from different depths and (**e**) Porayar core sediments. The sediments from both the cores show almost flat UCC normalized LREE and HREE pattern and slight enrichment of MREE including Eu. This implies that the sediments have been derived from less differentiated source in comparison to the UCC.

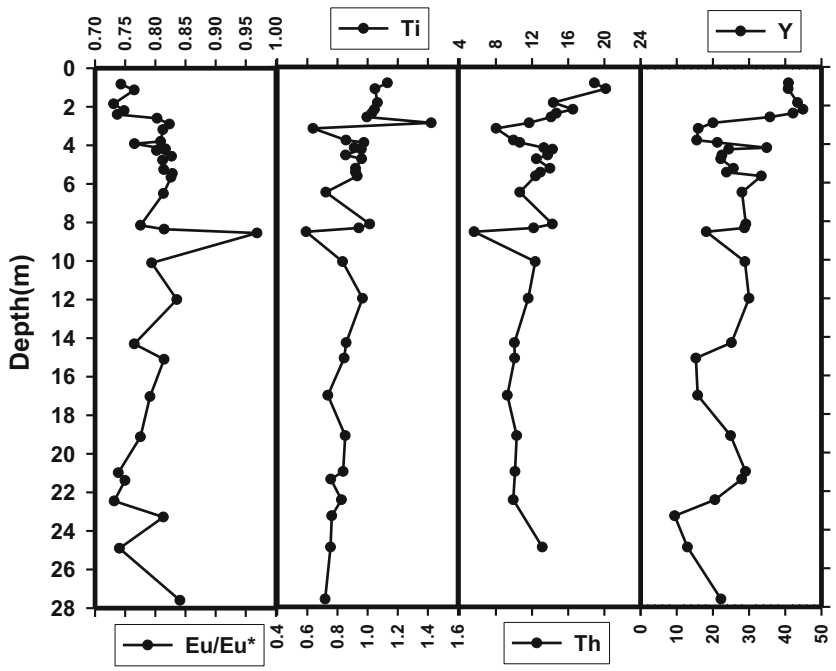

Figure 11. The depth wise variation trend of Th, Y and Ti with that of the Eu/Eu* for Uttrangudi sediments. The negative correlation of these elements with Eu/Eu* values mean that enrichment of heavy minerals such as titanite, allanite and monazite has resulted in relatively higher increase in LREE and HREE in comparison to Eu leading in decrease of Eu/Eu*.

It is observed that in both the cores, Eu/Eu* values show a significant negative correlation with the CIA values, particularly in Uttrangudi sediments. This would suggest that the Eu in sediments is modified to different extent by the process of weathering affecting its loss and lowering of Eu/Eu* values. Eu is known to be mobile in Eu^{2+} state, whereas it remains immobile in Eu^{3+} state. Thus, during weathering Eu can get mobilized by chemical breakdown of feldspar only if the local

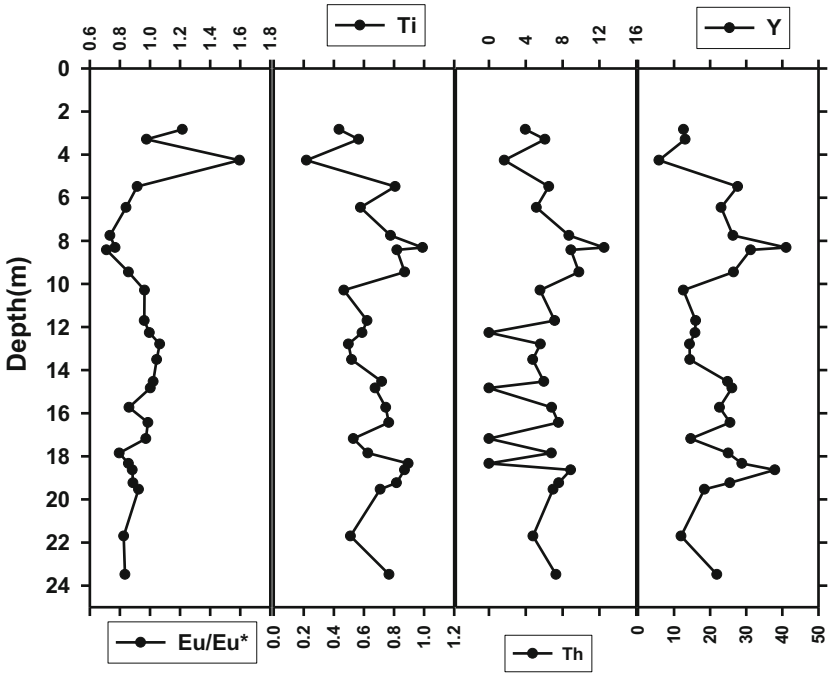

Figure 12. The depth-wise variation trend of Th, Y and Ti with that of the Eu/Eu* for Porayar sediments.

environment has been reducing. But it is known that even if mobilized during weathering of rocks, the REEs get redistributed within the soil profile (Nesbit 1979). Further, on erosion the re-mixing of soil results in values similar to rock (Cullers *et al.* 1987). There is other possibility that Eu mobilizes from sediments after their deposition. This would imply post-depositional weathering of feldspar under subsurface reducing conditions, where Eu^{3+} after their release reduce to Eu^{2+} and carried away by groundwater in a dissolved state. The UCC normalized REE pattern of both the cores (figure 10) shows almost flat LREE and HREE pattern and slight enrichment of MREE including Eu. This implies that the sediments have been derived from a less differentiated source in comparison to the UCC. It is further observed that the Uttrangudi sediments show variation in terms of Ce in UCC normalized plots (figure 10) and this can be distinguished into two groups; one without Ce anomaly and the other exhibiting slight positive Ce anomaly (figure 10). The development of positive Ce anomaly in sediments also suggests post-depositional weathering (Braun *et al.* 1998; Dia *et al.* 2000; Mayumi and Tasuku 2008). The preferential leaching of REEs other than Ce in a weathering profile could result in development of positive Ce anomaly (Marsh 1991). Similar observation has been made by Tripathi and Rajamani (2007) in river sediments. Thus, the variation particularly in Eu and Ce, between the two cores is due to post-depositional changes. The Uttrangudi sediments may have suffered more alteration in comparison to the Porayar sediments because of their older age and slower rate of deposition. Except the topmost ∼7 m samples, rest of the sediments in Uttrangudi are of upper mid Pleistocene, whereas almost entire sediments in Porayar core are of Holocene age. Further, the control of heavy minerals on Eu/Eu* value was evaluated. In the present study, the trace elements Th, Y and Ti are found to be associated with the REE bearing heavy minerals such as Monazite, Allanite and Titanite. For this, the depth-wise variation trend of Th, Y and Ti with that of the $(Eu/Eu^*)_N$ was plotted (figures 11 and 12). It is observed that like CIA, the above set of trace elements also exhibit negative correlation with $(Eu/Eu^*)_N$ values. This suggests that enrichment of heavy minerals has resulted in relatively higher values in LREE and HREE in comparison to Eu that is dominantly held in feldspars which has resulted in decrease in value of Eu/Eu*.

Thus, it is observed that Eu anomaly of sediments in the present study has been modified both by the variation in heavy mineral concentration and the weathering variability. The overall lower value of Eu/Eu* in Uttrangudi sediments in comparison to Porayar sediments may be due to higher degree of weathering exhibited by Uttrangudi

sediments. This may partly be because of post-depositional changes as the Uttrangudi sediments are older (upper Pleistocene) for most of the part. Thus, in absence of these changes it is expected that the sediments plot above their present position in $(Eu/Eu^*)_N$ vs. $(Gd/Yb)_N$ diagram (figure 8).

6. Conclusion

Primarily, the REEs in the studied sediments from Uttrangudi and Porayar areas of Cauvery delta are concentrated in silt and clay fraction and the varying percentage of sand acts as a diluting agent for them. The heavy mineral phases, along with the mafic minerals have largely controlled the REE concentration and pattern in the sediments from both the studied locations. The relation of Eu and CIA, complemented by positive Ce* anomaly on normalizing by UCC in various samples, particularly in Uttrangudi site indicates that the sediments have undergone post-depositional weathering changes.

Thus, the study reveals that REEs should be studied as a separate entity for the complexity of REE mobility and Eu and Ce anomalies and the REE-hosting minerals should always be studied keeping weathering conditions in view.

Acknowledgements

We thank DST, New Delhi for the financial assistance in the form of a research grant (No. SR/S4/ES-21/Cauvery/P1) to PS and JRF/SRF to the first author and for analytical support from DST FIST, facility to the Department of Earth Sciences, Pondicherry University. The authors are thankful to two anonymous reviewers for their valuable suggestions, which helped in improving the quality of the manuscript.

References

Alappat L, Tsukamoto S, Singh P, Srikanth D, Ramesh R and Frechen M 2010 Chronology of cauvery delta sediments from shallow subsurface cores using elevated-temperature Post-IR IRSL dating of feldspar. *Geochronometria* **37** 37–47.

Alvarez N C and Roser B P 2007 Geochemistry of black shales from the Lower Cretaceous Paja Formation, Eastern Cordillera, Colombia: Source weathering, provenance, and tectonic setting; *J. South Am. Earth Sci.* **23** 271–289.

Balachandran S, Asokan R and Sridharan S 2006 Global surface temperature in relation to northeast monsoon rainfall over Tamil Nadu; *J. Earth Syst. Sci.* **115** 349–362.

Bhaskar R Y J, Chetty T R K, Janardhan A S and Gopalan K 1996 Sm–Nd and Rb–Sr ages and P–T history of the Archean Sittampundi and Bhavani layered meta-anorthosite complexes in Cauvery shear zone, south India: Evidence for Neoproterozoic reworking of Archean crust; *Contrib. Mineral. Petrol.* **125** 237–250.

Bi L, Yang S, Zhao Y, Wang Z, Dou Y, Li C and Zheng H 2017 Provenance study of the holocene sediments in the Changjiang (Yangtze river) estuary and inner shelf of the east china sea; *Quat. Int.* **441** 147–161.

Braun J J, Viers J, Dupré B, Polve M, Ndam J and Muller J 1998 Solid/liquid REE fractionation in the lateritic system of Goyoum, East Cameroon: The implication for the present dynamics of the soil covers of the humid tropical regions; *Geochim. Cosmochim. Acta* **62** 273–299.

Chadwick B, Ramakrishnan M and Viswanatha M N 1981 Structural and metamorphic relations between Sargur and Dharwar supracrustal rocks and peninsular Gneisses in central Karnataka; *J. Geol. Soc. India* **22** 557–569.

Chadwick B, Vasudev V N and Hedge G V 2000 The Dharwar craton, southern India, interpreted as the result of Late Archaean oblique convergence; *Precamb. Res.* **99** 91–111.

Clift P D 2016 Assessing effective provenance methods for fluvial sediment in the South China Sea; *J. Geol. Soc. London, Spec. Publ.* **429** 9–29.

Cullers R L 1988 Mineralogical and chemical changes of soil and stream sediment formed by intense weathering of the Danberg granite, Georgia, USA; *Lithos* **21** 301–314.

Cullers R L 2000 The geochemistry of shales, siltstones and sandstones of Pennsylvanian–Permian age, Colorado, USA: Implications for provenance and metamorphic studies; *Lithos* **51** 181–203.

Cullers R L, Barrett T, Carlso R and Robinson B 1987 Rare-earth element and mineralogical changes in Holocene soil and stream sediment: A case study in the Wet Mountains, Colorado, USA; *Chem. Geol.* **63** 275–297.

Dia A, Gruau G, Olivié L G, Riou C, Molenat J and Curmi P 2000 The distribution of rare earth elements in groundwaters: Assessing the role of source-rock composition, redox changes and colloidal particles; *Geochim. Cosmochim. Acta* **64** 4131–4151.

Dixon J B, Weed S B, Kittrick J A, Milford M H and White J I 1977 Minerals in soil environments; *Soil Sci. Lett.* **248** 426–437.

Dou Y, Yang S, Shi X, Clift P D, Liu S, Liu J, Li C, Bi L and Zhao Y 2016 Provenance weathering and erosion records in southern Okinawa Trough sediments since 28 ka: Geochemical and Sr–Nd–Pb isotopic evidences; *Chem. Geol.* **425** 93–109.

Frallick P N and Kronberg B I 1997 Geochemical discrimination of clastic sedimentary rock sources; *Sedim. Geol.* **113** 111–124.

Gouveia M A, Prudencio M I and Figueiredo M O *et al.* 1993 Behavior of REE and other trace and major elements during weathering of granitic rocks, Evora, Portugal; *Chem. Geol.* **107** 293–296.

Hardy R G and Tucker M E 1988 X-ray powder diffraction of sediments. *Tech. Sedimentol.* 191–228.

Harris N B W, Santhosh M and Taylor P N 1994 Crustal evolution in South India. Constraints from Nd isotopes; *J. Geol.* **10** 139–150.

Hassan S, Ishiga H, Roser B P, Dozen K and Naka T 1999 Geochemistry of Permian–Triassic shales in the Salt Range, Pakistan: Implications for provenance and tectonism at the Gondwana margin; *Chem. Geol.* **158** 293–314.

Henderson P 1984 General geochemical properties and abundances of the rare earth elements; In: *Rare Earth Element Geochemistry* (ed) Henderson P, Elsevier, Oxford, 510p.

Huang J, Wan S, Xiong Z, Zhao D, Liu X, Li A and Li T 2016 Geochemical records of Taiwan-sourced sediments in the South China Sea linked to Holocene climate changes; *Palaeogeogr. Palaeoclimatol. Palaeoecol.* **44**1 871–881.

Huntsman M P, Tiercelin J J, Benoit M, Ringrose S, Diskin S, Cotton J and Hemond C 2009 Sediment geochemistry and tectonic setting: Applictaion of discrimnatation diagrams to early stages of intra-continental rift evolution, with examples from the Okavango and Southeren Tanganyika rift basins; *J. Earth Sci.* **53** 33–44.

Jayananda M, Moyen J F, Martin H, Peucat J J, Auvray B and Mahabaleswar B 2000 Late Archaean (2550–2520 Ma) juvenile magmatism in the Eastern Dharwar geochemistry; *Precamb. Res.* **99** 225–254.

Jin L, Ma L, Dere A, White T, Mathur R and Brantley S L 2017 REE mobility and fractionation during shale weathering along a climate gradient; *Chem. Geol.* **466** 352–379.

Krogstad E J, Hanson G N and Rajamani V 1991 U–Pb ages of zircon and sphene for two gneiss terrains adjacent to the Kolar Schist Belt, south India: Evidence for separate crustal evolution histories; *J. Geol.* **99** 801–816.

Maharana C, Srivastava D and Tripathi J K 2018 Geochemistry of sediments of the peninsular rivers of the Ganga basin and its implication to weathering, sedimentary processes and provenance; *Chem. Geol.* **483** 1–20.

Marsh J S 1991 REE fractionation and Ce anomalies in weathered Karoo dolerite; *Chem. Geol.* **90** 189–194.

Mayumi S and Tasuku A 2008 Chemical condition for the appearance of a negative Ce anomaly in stream waters and groundwaters; *Geochem. J.* **42** 371–380.

McLennan S M 1989 Rare earth elements in sedimentary rocks: Influence of provenance and sedimentary processes; In: Geochemistry and Mineralogy of Rare Earth Elements (eds) B R Lipin and G A McKay, *Rev. Mineral.* **21** 169–200.

McLennan S M, Taylor S R, McCulloch M T and Maynard J B 1990 Geochemical and Nd–Sr isotopic composition of deep-sea turbidites: Crustal evolution and plate tectonic associations; *Geochim. Cosmochim. Acta* **54** 2015–2050.

Meissner B, Deters P, Srikantappa C and Kohler H 2002 Geochronological evolution of the Moyar, Bhavani and Palghat shear zones of southern India: Implication of east Gondwana correlations; *Precamb. Res.* **114** 149–175.

Nesbitt H W 1979 Mobility and fractionation of rare earth elements during weathering of a granodiorite; *Nature* **279** 206–210.

Nesbitt H W and Young G M 1982 Early Proterozoic climates and plate motions inferred from major element chemistry of lutites; *Nature* **299** 715–717.

Nesbitt H W and Young G M 1996 Petrogenesis of sediments in the absence of chemical weathering: Effects of abrasion and sorting on bulk composition and mineralogy; *Sedimentology* **43** 341–358.

Nesse W D, Ohlander B, Land M, Ingri J and Widerlund A 1996 Mobility of rare earth elements during weathering of till in northern Sweden: Introduction to minerology; *Appl. Geochem.*, Oxford University Press, New York **11** 93–99.

Radhakrishna B P 1983 Archaean granite-greenstone terrain of south Indian shield; In: *Precambrian of South India* (eds) Naqvi S M and Rogers J J W, *Geol. Soc. India Memoir* **4** 1–46.

Raith M M, Srikantappa C, Buhl D and Koehler H 1999 The Nilgiri enderbites, south India: Nature and age constraint on protolith formation, high-grade metamorphism and cooling history; *Precamb. Res.* **98** 129–150.

Rajesh H M 2012 A geochemical perspective on charnockite magmatism in peninsular India; *Geosci. Front.* **3(6)** 773–788.

Sadakata N 1980 Boring data and fossil pollen analysis in the Cauvery delta, south India; In: *Geog. Field Res. India*, Hiroshima University Special, **8** 175–179.

Saini N K, Mukherjee P K, Rathi M S, Khanna P P and Purohit K K 1998 A new geochemical reference sample of granite (DG-H) from Dalhousie, Himachal Himalaya; *J. Geol. Soc. India* **52** 603–606.

Santosh M, Maruyama S and Sato K 2009 Anatomy of a Cambrian suture in Gondwana: Pacific-type orogeny in southern India? *Gondwana Res.* **16(2)** 321–341.

Shapiro L and Brannock W W 1962 Rapid analysis of silicate, carbonate, and phosphate rocks; *US Geol. Surv. Bull.* **1144A** 1–56.

Sharma A and Rajamani V 2000a Major element, REE, and other trace element behavior in amphibolite weathering under semiarid conditions in southern India; *J. Geol.* **108** 487–496.

Shou Y Y, Hoi S J, Man S C and Cong X L 2002 The rare earth element compositions of the Changjiang (Yangtze) and Huanghe (Yellow) river sediments; *Earth Planet. Sci. Lett.* **201** 407–419.

Singh P and Rajamani V 2001 REE geochemistry of recent clastic sediments from the Kaveri floodplains, southern India: Implication to source area weathering and sedimentary processes; *Geochim. Cosmochim. Acta* **65** 3093–3108.

Singh P, Yadava M G, Ahmad M Z, Mohapatra P P, Laskar A H, Doradla S and Kumanan C J 2015 Fertile farmlands in Cauvery delta: Evolution through LGM; *Curr. Sci.* **108** 218–225.

Srikanth D 2012 Geochemical and carbon isotope studies on the surface and subsurface sediments of Cauvery Delta, South India; Unpubl. Ph.D Thesis, Pondicherry University, Pondicherry.

Stuiver M and Reimer J 1993 Extended ^{14}C data base and revised CALIB 3.0 ^{14}C calibration program; *Radiocarbon* **35** 215–230.

Swaminath J and Ramakrishnan M 1981 Early Precambrian supracrustals of southern Karnataka: Present classification and correlation; *Geol. Soc. India Memoir* **112** 23–38.

Swaminath J, Ramakrishnan M and Viswanatha M N 1976 Dharwar stratigraphic model and Karnataka craton evolution; *Rec. Geol. Surv. India* **107** 149–175.

Taylor S R and McLennan S M 1985 *The Continental Crust: Its Composition and Evolution*; Blackwells, Oxford, 312p.

Tripathi J K and Rajamani V 2003 Geochemistry of Delhi quartzites: Implications for the provenance and source area weatherin; *J. Geol. Soc. India* **62** 215–226.

Tripathi J K and Rajamani V 2007 Geochemistry and origin of ferruginous nodules in weathered granodoiritic gneisses, Mysore Plateau, southern India; *Geochim. Cosmochim. Acta* **7** 1674–1688.

Valdiya K S 1998 Late Quaternary movements and landscape rejuvenation in southern Karnataka and adjoining Tamil Nadu in southern Indian Shield; *J. Geol. Soc. India* **51** 139–166.

Vázquez O A, Perdrial J, Harpold A, Zapata R X, Rasmussen C, McIntosh J, Schaap M, Pelletier J D, Brooks P D, Amistadi M K and Chorover J 2015 Rare earth elements as reactive tracers of biogeochemical weathering in forested rhyolitic terrain; *Chem. Geol.* **391** 19–32.

Vital H, Stattegger K and Garbe-Schoenberg C D 1999 Composition and trace-element geochemistry of detrital clay and heavy-mineral suites of the lowermost Amazon River: A provenance study; *J. Sedim. Res.* **69** 563–575.

Wronkiewicz D J and Condie K C 1987 Geochemistry of Archean shales from the Witwatersrand Supergroup, South Africa: source-area weathering and provenance; *Geochim. Cosmochim. Acta* **51** 2401–2416.

Zhao D, Wan S, Toucanne S, Clift P D, Tada R, Révillon S and Jiang H 2017 Distinct control mechanism of fine-grained sediments from Yellow River and Kyushu supply in the northern Okinawa T rough since the last glacial; *Geochem. Geophys. Geosyst.* **18(8)** 2949–2969.

Zhao D, Wan S, Clift P D, Tada R, Huang J, Yin X and Li A 2018 Provenance, sea-level and monsoon climate controls on silicate weathering of Yellow River sediment in the northern Okinawa Trough during late last glaciation; *Palaeogeogr. Palaeoclimatol.* **490** 227–239.

Corresponding editor: Santanu Banerjee